

# Detecting extreme mass ratio inspiral events in LISA data using the Hierarchical Algorithm for Clusters and Ridges (HACR)

Jonathan Gair\*

*Institute of Astronomy, University of Cambridge, Madingley Road, Cambridge, CB3 0HA, UK*

Gareth Jones

*Cardiff School of Physics and Astronomy, Cardiff University,*

*Queens Buildings, The Parade, Cardiff, CF24 3AA, UK*

(Dated: December 2, 2024)

One of the most exciting prospects for the Laser Interferometer Space Antenna (LISA) is the detection of gravitational waves from the inspirals of stellar-mass compact objects into supermassive black holes. Detection of these sources is an extremely challenging computational problem due to the large parameter space and low amplitude of the signals. However, recent work has suggested that the nearest extreme mass ratio inspiral (EMRI) events will be sufficiently loud that they might be detected using computationally cheap, template-free techniques, such as a time-frequency analysis. In this paper, we examine a particular time-frequency algorithm, the Hierarchical Algorithm for Clusters and Ridges (HACR). This algorithm searches for clusters in a power map and uses the properties of those clusters to identify signals in the data. We find that HACR applied to the raw spectrogram performs poorly, but when the data is binned during the construction of the spectrogram, the algorithm can detect typical EMRI events at distances of up to  $\sim 2.5$  Gpc. This is a little further than the simple Excess Power method that has been considered previously. We discuss the HACR algorithm, including tuning for single and multiple sources, and illustrate its performance for detection of typical EMRI events, and other likely LISA sources, such as white dwarf binaries and supermassive black hole mergers. We also discuss how HACR cluster properties can be used for parameter extraction.

PACS numbers: 04.25.Nx,04.30.Db,04.80.Cc,04.80.Nn,95.55.Ym,95.85.Sz

## I. INTRODUCTION

Astronomical observations indicate that many galaxies host a supermassive black hole (SMBH) in their centre, which is surrounded by a cluster of stars. Stellar encounters in the cluster perturb stellar orbits and can put objects onto trajectories that pass very close to the SMBH. The orbit loses energy and angular momentum to a burst of gravitational radiation emitted near periaapse, which may leave the object bound to the central black hole. Gravitational radiation dominates the subsequent evolution, and the object gradually inspirals into the SMBH. If the captured star is a compact object, i.e., a white dwarf, neutron star or black hole, (so that it is not tidally disrupted) and the SMBH has mass  $M \sim \text{few} \times 10^5 M_\odot - 10^7 M_\odot$ , the gravitational waves (GWs) emitted during the last several years of inspiral will be at frequencies that the planned space-based gravitational wave (GW) observatory LISA will be able to detect.

The rate at which these extreme mass ratio inspiral (EMRI) events occur in the Universe is highly uncertain, but is likely to be only a few times per year in each  $\text{Gpc}^3$  of space [1, 2]. The closest events are, therefore, likely to be at distances of 1 Gpc and will have typical instantaneous strain amplitudes of  $h \sim 10^{-22}$ . This must be compared to the characteristic noise strain in the LISA detector of  $\sim 5 \times 10^{-21}$  at the floor of the noise curve near 5 mHz [3, 4]. LISA EMRI events will therefore be buried in the instrumental noise. However, the EMRI waveforms will be detectable for several years before plunge, and detection is therefore possible by building up the signal-to-noise ratio over many waveform cycles. The optimal method for the detection of a known time series signal  $h(t)$  embedded in stationary Gaussian noise  $n(t)$  is matched filtering, i.e., computing the correlation of the data stream with the waveform template  $h(t)$ , weighted by the noise variance of the detector. Matched filtering requires the existence of a bank of templates that describe all possible signals that might be present in the data. Typical EMRI signals are complicated since the orbits are eccentric and inclined with respect to the equatorial plane of the SMBH, which leads to the presence of various modulations in the waveform. An EMRI waveform depends on 17 parameters (although several of these are not important for determining the waveform phasing) and LISA will detect up to  $\sim 10^5$  cycles of the waveform prior to plunge. Estimating that one template might be required per cycle in each parameter, and  $\sim 6$  important parameters, gives an estimate of  $10^{30}$  templates required for the simplest case of a search for a single

---

\* email address: jgair@ast.cam.ac.uk

EMRI embedded in pure Gaussian noise. This is far more than can be searched in a reasonable computational time.

Analysis of LISA data is made even more complicated by the fact that it is signal dominated, i.e., at any moment the data stream includes not only instrumental noise but thousands of signals of different types which overlap in time and frequency. The optimal matched filter should therefore be a superposition of all the signals that are present. Techniques exist to construct such a global matched filter iteratively, such as Markov Chain Monte Carlo methods, and are currently being investigated in the context of LISA [5, 6, 7], including for characterisation of LISA EMRIs [8]. However, these methods are also computationally intensive, and it is not yet clear that they will converge in a reasonable time unless some advance estimate has been made of the parameters of the signals present in the data stream. To devise such parameter estimation techniques, it is reasonable to first consider the problem of detecting a single source in noisy data, before using and adapting the methods to the case of multiple sources.

As described above, it is not possible to use fully coherent matched filtering to detect a single EMRI in LISA data since the computational cost of searching through the many templates is too high. However, one alternative is to use a semi-coherent approach — rather than search for the full waveform, begin with a coherent search for  $\sim 2\text{--}3$  week segments of EMRI waveforms, before following up with a second stage where the power in each segment is summed up through sequences of segments that correspond to inspirals. An analysis [2] suggested that, with reasonable computational resources, this technique could detect individual EMRI events out to a redshift  $z \approx 1$ , which would mean as many as several thousand EMRI detections over the duration of the LISA mission, although this is very dependent on the intrinsic astrophysical rate of EMRI events. The semi-coherent method, although computationally feasible, makes heavy use of computing resources. On the other hand, the large potential event rate suggests that it might be possible to detect the loudest several EMRI events using much simpler, template-free techniques, at a tiny fraction of the computational cost.

One promising approach for the detection of EMRIs, and other types of LISA sources, is a time-frequency analysis, i.e., divide the LISA data stream into shorter segments, perform a Fourier analysis of each, thus constructing a time-frequency spectrogram of the data, and then search this time-frequency map for features. The simplest possible time-frequency algorithm is an excess power search, i.e., a search for unusually bright pixels in the spectrogram. While this performs poorly when applied to the raw spectrogram, if the data is binned first, the excess power method is able to detect typical EMRI events at distances of up to  $\sim 2.25\text{Gpc}$  [9, 10], or about half the distance of the semi-coherent search [2]. The disadvantage of the excess power method in isolation is that it does not provide much information about the source parameters, but merely indicates that a source is present in the data. A follow up analysis must therefore be done in order to extract information about the excess power events [11].

In this paper we consider a somewhat more sophisticated time-frequency algorithm, the Hierarchical Algorithm for Clusters and Ridges (HACR) [12]. This method involves first identifying unusually bright pixels in the time-frequency map, then constructing a cluster of bright pixels around it, before finally using the number of pixels in the cluster as a threshold to distinguish signals from noise events. If the pixel threshold is set to 1, the HACR search becomes equivalent to the Excess Power search. The properties of the HACR clusters encode information about the source, and thus in a single analysis HACR allows both detection and parameter estimation.

We have found that when HACR is applied to the unbinned spectrogram, it performs poorly, but if the spectrogram is first binned via the same technique used for the Excess Power search [9, 10], we find that HACR outperforms the Excess Power search, as we would expect. HACR is able to detect typical EMRI events at distances of  $\sim 2.5\text{Gpc}$ , which is only a little further than the Excess Power technique. However, the HACR clusters associated with detection events tend to have several hundred pixels, and thus encode a significant amount of information about the source. The HACR search can be tuned for specific sources at specific distances, or for specific sources at arbitrary distance, or for multiple types of source at multiple distances. While the detection performance for a specific source does depend on how the HACR thresholds are tuned, we find that the variation of detection rate is not huge and so a single HACR search could be used to detect multiple types of event in a search of the LISA data. Since the HACR search encompasses the Excess Power search as a subset, we will compare HACR's performance with the performance of the Excess Power algorithm throughout this paper.

The paper is organised as follows. In Section II we describe LISA, the LISA data stream and LISA sources, including the waveform models we use for source injections and the noise model we use to estimate LISA's noise spectral density. In Section III we introduce the HACR algorithm, discuss how the time-frequency map may be binned to improve detection of signals and describe how the HACR search can be characterised when no signals are present. In Section IV, we describe how the HACR thresholds may be tuned for detection of a single source or multiple sources, while maintaining a constant overall false alarm probability, and we evaluate HACR's performance at detecting a range of EMRI signals in LISA data. Although EMRIs are the main focus of our analysis, time-frequency techniques like HACR may play a role in the detection and identification of other sources in the LISA data stream. For this reason, in Section V we evaluate HACR's performance at detecting other classes of signal, specifically the gravitational waves from white dwarf binaries and the mergers of supermassive black hole binaries. In Section VI we will briefly describe how the properties of the event candidate identified by HACR could be used to estimate

parameters of the source, although a more detailed investigation of this is reserved for a future paper. Finally, in Section VII we summarise our results.

## II. LISA OVERVIEW — DETECTOR AND SOURCES

### A. The LISA mission

The LISA detector will consist of three spacecraft in heliocentric Earth-trailing orbits, 5 million kilometres apart at the corners of an (approximately) equilateral triangle (see [13] for a full description of the mission). There will be two lasers running between each pair of spacecraft, one in each direction, and it is the differences in laser phase between the various light travel paths that indicate that gravitational waves are passing through the detector. In the raw data, the laser phase difference is totally dominated by laser frequency noise. However, this can be suppressed without eradicating the GW signal using Time Delay Interferometry (TDI, see for instance [14] and references therein). At high frequencies, there are three independent TDI channels in which the noise is uncorrelated, which are typically denoted  $A$ ,  $E$  and  $T$ . At low frequencies there are essentially only two independent data channels, since LISA can be regarded as a superposition of two static orthogonal Michelson interferometers over relevant timescales. These two low frequency response functions, denoted  $h_I$  and  $h_{II}$ , are defined in [3]. In this analysis we treat the LISA data stream as consisting of only the latter two channels, since our sources are at comparatively low frequency, and the Michelson responses are quick and easy to compute. While not a totally accurate representation of LISA, this approach incorporates the modulations due to the detector motion in a reasonable way and so is sufficient for the qualitative nature of the current analysis.

LISA is expected to detect gravitational waves from many sources of several different types. LISA should detect many millions of compact object binaries (white dwarf – white dwarf, white dwarf – neutron star, neutron star – neutron star) in our own galaxy, which generate essentially monochromatic gravitational wave signals (modulo detector modulations). These binary signals are sufficiently dense in frequency space that the majority will not be individually resolvable, but form a confusion foreground from which other sources must be extracted. However, several thousand binaries will still be resolvable [13]. LISA should also detect several (estimates suggest as many as a few tens per year, e.g., [15]) signals from the final inspiral and merger of SMBH binaries. For SMBHs of appropriate mass,  $M \sim 10^4 M_\odot - 10^7 M_\odot$ , these mergers will be visible out to very high redshifts and will appear in the LISA data stream with very high signal-to-noise ratios. Over the course of its planned three year mission, LISA should also detect as many as several hundred EMRI events as discussed in the introduction, and may detect bursts from astronomical events and perhaps a stochastic GW background.

### B. A typical EMRI source

In this paper we concentrate on the issue of detection of EMRI events and to do so we must consider a typical EMRI signal. Work on the semi-coherent search suggested that the LISA EMRI event rate would be dominated by the inspiral of black holes of mass  $m \sim 10 M_\odot$  into SMBHs with mass  $M \sim 10^6 M_\odot$  [2]. The EMRI will be detectable for the last several years of the inspiral, and hence could last for a significant fraction of the LISA mission duration. Moreover, since the EMRI will typically be captured with very high eccentricity and random inclination with respect to the equatorial plane of the SMBH, the inspiral orbit is likely to have some residual eccentricity and inclination at plunge. Theoretical models [16] and some observational evidence [17, 18] indicate that most astrophysical black holes will have significant spins. Bearing all this in mind, we chose as a “typical” EMRI event (which we shall refer to as source “A”) the inspiral of a  $10 M_\odot$  black hole into a  $10^6 M_\odot$  SMBH with spin  $a = 0.8M$ . We assumed conservatively that the LISA mission will last only three years ( $3 \times 2^{25}$ s) and that the EMRI event was observed for the whole of the LISA mission, but plunged shortly after the end of the observation. This set the initial orbital pericentre to be at  $r_p \approx 11M$ . We took the eccentricity and orbital inclination at the start of the observation to be  $e = 0.4$  and  $\iota = 45^\circ$  and fixed the sky position in ecliptic coordinates to be  $\cos\theta_S = 0.5$ ,  $\phi_S = 1$ . The orientation of the SMBH spin was chosen such that if the SMBH was at the Solar System Barycentre, the spin would point towards ecliptic coordinates  $\cos(\theta_K) = -0.5$ ,  $\phi_K = 4$ . These latter orientation angles were chosen arbitrarily, but are non-special. The EMRI waveform was generated using the approximate, “kludge”, approach described in [19, 20]. These kludge waveforms are much quicker to generate than accurate perturbative waveforms, but capture all the main features of true EMRI waveforms and show remarkable faithfulness when compared to more accurate waveforms. In addition to source “A”, we considered two other EMRI injections. These had the same parameters as “A”, except for the initial orbital eccentricity, which was taken to be  $e = 0$  for source “K” and  $e = 0.7$  for source “N”. The waveforms and

waveform labels used are the same as those examined in the context of the Excess Power search in [10], to facilitate comparison.

In section V, we also examine the performance of HACR in detecting other LISA sources, namely white dwarf binaries and SMBH mergers. For both of these sources, we take the waveform model, including detector modulations, from [3]. Although more sophisticated SMBH merger models are available, the prescription in [3] is sufficiently accurate for our purposes. The waveform model for a non-evolving white dwarf binary is very simple and has been well understood for many years and is summarised in [3].

### C. Modelling LISA’s noise spectral density

To characterize the search, we need to include the effects of detector noise. To do this, we use the noise model from Barack and Cutler [4]<sup>1</sup>, which includes both instrumental noise and “confusion noise” from the unresolvable white dwarf binary foreground. The noise spectral density is given by

$$S_h(f) = \min \left\{ S_h^{inst}(f) \exp(\kappa T_{mission}^{-1} dN/df), S_h^{inst}(f) + S_h^{gal}(f) \right\} + S_h^{ex.gal}(f) \quad (2.1)$$

$$\text{where } S_h^{inst}(f) = 9.18 \times 10^{-52} f^{-4} + 1.59 \times 10^{-41} + 9.18 \times 10^{-38} f^2 \text{Hz}^{-1} \quad (2.2)$$

$$\text{and } S_h^{gal}(f) = 50 S_h^{ex.gal}(f) = 2.1 \times 10^{-45} \left( \frac{f}{1 \text{Hz}} \right)^{-7/3} \text{Hz}^{-1}. \quad (2.3)$$

In this, the parameter  $\kappa T_{mission}^{-1}$  measures how well white dwarfs of similar frequency can be distinguished, and we take  $\kappa T_{mission}^{-1} = 1.5/\text{yr}$  as in [4]. In practice, rather than adding coloured noise to the injected signal, we first whiten the signal using this theoretical noise prescription and then inject it into white Gaussian noise. The procedures are equivalent, under the assumption that the LISA data stream can be regarded as stationary and supposing that the noise spectral density is known or can be determined. This is likely to be a poor assumption, but a more accurate analysis is very difficult and beyond the scope of this paper.

## III. THE HIERARCHICAL ALGORITHM FOR CLUSTERS AND RIDGES

### A. Description of method

The HACR algorithm is used to identify and subsequently cluster together pixels containing excess power in a time-frequency map and represents a slight modification to the TFClusters algorithm [21].

In a given time-frequency map, we denote the power in a pixel as  $P_{i,j}$  where  $i$  and  $j$  are the time and frequency co-ordinates of the pixel. HACR classifies pixels satisfying  $P_{i,j} > \eta_{up}$  as *black pixels*. This first stage of thresholding provides a quick first search through the data identifying pixels with significant excess power which may be members of larger clusters of pixels that represent GW events. Pixels sharing an edge or corner with an existing black pixel are classified as a *grey pixel* if they satisfy  $P_{i,j} > \eta_{low}$ . All pixels which may be connected to a black pixel through a path of touching grey pixels are evaluated to see whether they themselves should be classified as grey. This process is repeated and HACR builds clusters of grey pixels around each black pixel identified during the first stage of thresholding. To be classified as an *event candidate* a cluster of pixels must satisfy  $N_c > N_p$  where  $N_c$  is the number of pixels contained in a particular cluster. When using HACR we therefore have to specify three thresholds:  $\eta_{up}$ ,  $\eta_{low}$  and  $N_p$ . The algorithm is illustrated in Figure 1

There is some degeneracy between the choice of the  $\eta_{low}$  and  $N_p$  thresholds since  $\eta_{low}$  determines the size of a cluster of pixels and  $N_p$  decides whether the cluster is large enough to be considered an event candidate. Choosing a low value of  $\eta_{low}$  will tend to make clusters larger, but this can be compensated for by using a larger value for the pixel threshold,  $N_p$ . There is thus a degeneracy between these two thresholds. In order to reduce the dimensionality of our parameter space we will fix the value of  $\eta_{low}$  during our analysis and concentrate only on tuning the values of  $\eta_{up}$  and  $N_p$ . In order to avoid constricting the search unnecessarily we set  $\eta_{low}$  to its lowest possible value throughout our analysis, thereby maximising the size of any cluster.

---

<sup>1</sup> NB The published version of this paper contains an error in the expression for  $S_h$ , which has been corrected in the preprint gr-qc/0310125. We use the corrected expressions here.

The approach of fixing  $\eta_{low}$  should be adequate for determining the detection rate of the HACR search, which is the main concern of the current paper. However, it will mean that clusters identified by HACR representing signal events will tend to include a reasonable number of noise pixels, which might affect parameter estimation algorithms of the type we discuss in Section VI. In a future paper, when we explore parameter extraction, we will examine more carefully how the choice of lower threshold affects the performance of parameter estimation algorithms.

### 1. Investigating “binning” of the time-frequency maps

It is possible to improve the performance of the search by “binning” our time-frequency maps through summing the power of individual pixels within a rectangular box. This binning procedure was the key stage of the simple Excess Power search discussed in [9, 10].

For a given source, the box size that will do best for detection will be large enough to include much of the signal power but small enough to avoid too much noise contribution. This optimum will be source specific due to the wide variation in EMRI waveforms. The inspiral of a  $0.6M_{\odot}$  white dwarf occurs much more slowly than that of a  $10M_{\odot}$  black hole, so in the first case, the optimal box size is likely to be longer in the time dimension. GWs from an inspiral into a rapidly spinning black hole or from a highly eccentric inspiral orbit are characterized by many frequency harmonics, often close together. In that case, a box that is wider in the frequency dimension may perform well. In designing a search, a balance must therefore be struck between having sensitivity to a range of sources and increasing the reach of the search for a specific source. We will consider this more carefully in Section IV B.

This binning allows us to construct an average power map for each box size. The average power contained within a box is defined by

$$P_{i,j}^{n,l} = \frac{1}{m} \sum_{a=0}^{n-1} \sum_{b=0}^{l-1} P_{i+a,j+b} \quad (3.1)$$

where  $n, l$  are the lengths of the box edges in the time and frequency dimensions respectively and  $m = n \times l$  is the number of data points enclosed. This average power is computed for a box aligned on each pixel in the time-frequency map. In practise, for ease of computation we choose the alignment so that the pixel is in the top left hand corner of

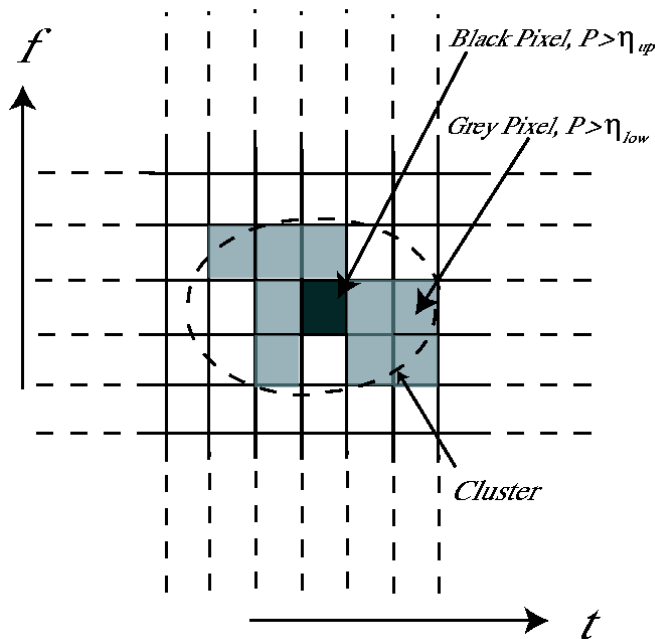


FIG. 1: A time-frequency map illustrating the HACR algorithm. Firstly, pixels with power  $P_{i,j} > \eta_{up}$  are classified as *black pixels*. Surrounding pixels with  $P_{i,j} > \eta_{low}$  are then classified as *grey pixels* building a cluster around the black pixel. Finally the cluster is classified as an event candidate if the number of pixels it contains,  $N_c$ , exceeds the threshold  $N_p$ .

the box. Adjacent pixels in the average power map are therefore not independent. As in [9], we use only box sizes  $(n, l) = (2^{n_t}, 2^{n_f})$  for all possible integer values of  $n_t$  and  $n_f$ . We denote the total number of different box shapes used as  $N_{box}$ .

## 2. Efficient “binning” method

The binned spectrograms for each box size can be generated in a particular sequence that improves the efficiency and speed of the search as shown in Figure 2. We first construct the unbinned ( $n = 1, l = 1$ ) map of the data and store it as map A. Before analysing map A we construct the ( $n = 1, l = 2$ ) map by summing the powers in vertically adjacent bins and storing this as map B (step 1). We then search map A using HACR before summing the power of pixels in horizontally adjacent bins to construct the ( $n = 2, l = 1$ ) map, and overwrite map A (step 2). Repeating this procedure on this new map A, we construct and search all the box sizes ( $n = 2^{n_t}, l = 1$ ). Before analysing the ( $n = 1, l = 2$ ) map stored as map B we construct the ( $n = 1, l = 4$ ) map and store this as map A (step 3). Using and overwriting map B, we construct and search all the box sizes ( $n = 2^{n_t}, l = 2$ ) (step 4). We repeat this procedure until we have searched all possible box sizes up to the limit imposed by the size of our time-frequency map.

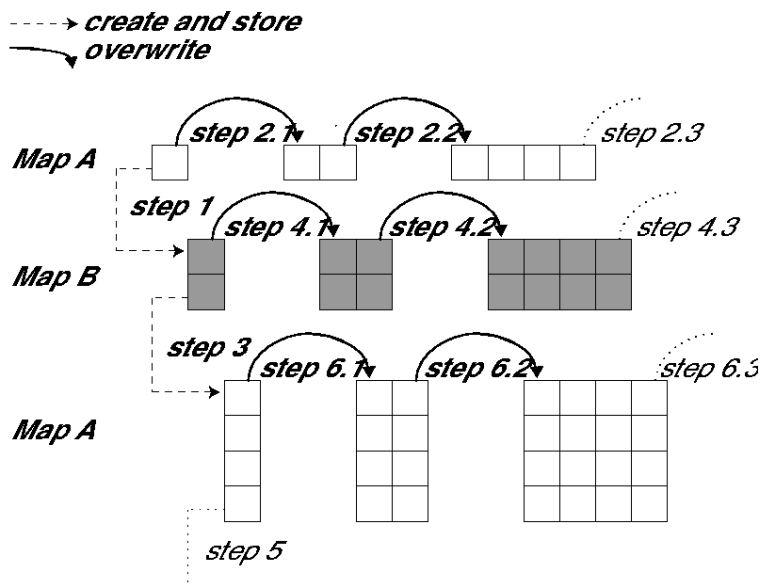


FIG. 2: Schematic showing the efficient binning of the time-frequency map. We begin with an unbinned spectrogram (Map A) which we use to construct the ( $n = 1, l = 2$ ) map (Map B) in step 1. Next we search Map A, recording results, before constructing the ( $n = 2, l = 1$ ) map in step 2.1. This method is repeated as we construct and search larger maps. This efficient binning method minimises the amount of computation required to create the maps and reduces the quantity of data we are required to store. See the efficient “binning” method section (III A 2) in the main text for a more detailed explanation.

Using this efficient binning method we are required to store only two time-frequency maps at a given time and reduce the number of binnings we need to perform through careful recycling of maps.

We set our thresholds separately for each box size and denote them  $\eta_{up}^{n,l}$  and  $N_p^{n,l}$  where the superscripts refer to the dimensions of the box size we are using. HACR has made a detection if both thresholds are exceeded by *at least one* cluster in *at least one* binned spectrogram.

To characterize the entire search (over all box sizes) we use the overall false alarm probability (*OFAP*). This is defined as the fraction of LISA missions in which HACR would make at least one false detection in at least one of the binned time-frequency maps, in the absence of any signals. We could allow each box size that we use to analyse our data to contribute a different amount to *OFAP*. However, to avoid prejudicing our results, we choose to assign an equal false alarm probability to each box size. We call this quantity the additional false alarm probability (*AFAP*). To be clear, *AFAP* is the probability of a false alarm in a particular box size, i.e., the fraction of LISA missions in which *that particular box size* would yield a false detection. The quantity *OFAP* is the overall false alarm probability

of the entire search, using the results from every box size, i.e.,  $OFAP$  is the fraction of LISA missions in which *at least one* box size would yield a false detection. The way in which the thresholds are computed ensures that each box size adds  $AFAP$  to the overall false alarm rate (hence “additional”), despite the fact that the binned spectrograms are not all independent. This will be described in Section IV A, and ensures that in practice  $OFAP = N_{box} * AFAP$ .

It is important to note that in the case  $N_p = 1$  then the HACR algorithm is equivalent to the Excess Power method described in earlier papers [9, 10]. A comparison between these two algorithms will be made several times in the subsequent sections of this paper.

### 3. Constructing spectrograms

In our study we considered a three year LISA mission, and used  $3 \times 2^{25}s$  of simulated LISA data sampled at  $0.125Hz$  (a cadence of  $8s$ ). To construct the time-frequency map, this data was divided into  $2^{20}s$  (2 week) sections, and an FFT was performed on each section. The resulting time-frequency spectrograms consist of 96 points in time and 65536 points in frequency giving us  $N_{box} = 7 \times 17 = 119$  possible box sizes of the form  $n = 2^{n_t}, l = 2^{n_f}$  where  $n_t = 0...6$  and  $n_f = 0...16$ .

A power spectrogram was constructed for both low-frequency channels,  $h_I$  and  $h_{II}$  (as described in II A), and these were summed pixel by pixel to produce the time-frequency map searched by the HACR algorithm. In practice, to include noise, we took the noise in the two LISA channels to be normal, gaussian and white and whitened the injected signals using the theoretical LISA noise curve described in Section II. In this approach, in the absence of a signal the power,  $P_{i,j}$ , in each pixel of the unbinned spectrogram will be distributed as a  $\chi^2$  with 4 degrees of freedom.

## B. Search characterisation

Tuning HACR is a two step process. Firstly, simulated noisy data is analysed in order to identify pairs of thresholds  $\eta_{up}^{n,l}$  and  $N_p^{n,l}$  which give rise to a given false alarm probability,  $AFAP$ , for each box size,  $n \times l$ . Secondly, a stretch of simulated data containing both noise and a signal is analysed using these pairs of thresholds and the detection rate (or probability) is measured. For each value of false alarm probability considered we can then choose the threshold pair which gives the largest detection rate. In this way, we obtain the optimum Receiver Operator Characteristic (ROC) curve for HACR for the detection of a particular source. Throughout the paper, we will use the terms detection *rate* and false alarm *probability* in order to make a distinction between event candidates caused by a signal or by noise. What we are really computing as the detection *rate* is the detection probability, i.e., the fraction of LISA missions in which a particular source would be detected if we had many realisations of LISA. A more relevant observational quantity is the fraction of sources of a given type in the Universe that would be detected in a *single* LISA observation. The population of LISA events will have random sky positions, plunge times and plunge frequencies. They therefore sample different parts of the time-frequency spectrogram, which to some extent mimics averaging over noise realisations. The detection rate can thus be taken as a guide to the fraction of sources similar to the given one that would be detected in the LISA mission. A more accurate assessment of the fraction of sources detected requires injection of multiple sources simultaneously, but we do not consider that problem here.

To characterize the noise properties of the search we used  $\sim 10000$  noise realisations and analysed them with the thresholds  $\eta_{up}^{n,l}$  and  $N_p^{n,l}$  set as low as is sensibly possible, recording the peak power,  $P_{max}$ , and size,  $N_c$ , of every cluster detected. With such a list of clusters, it is possible during post-processing to obtain the number of false alarm detections that would be made using any set of thresholds so long as  $\eta_{up} > (\eta_{up}^{n,l})_{min}$  and  $N_p > (N_p^{n,l})_{min}$ .

The minimal value of the pixel threshold is  $(N_p^{n,l})_{min} = 1$ . This means that any box with  $P_{i,j}^{n,l} > (\eta_{up}^{n,l})_{min}$  will be recorded at this stage. In principle, the minimal value of  $\eta_{up}^{n,l}$  is  $\eta_{low}^{n,l}$ , but for small box sizes this assignment leads to huge numbers of potential clusters being recorded. The value of  $\eta_{low}^{n,l}$ , although not independent of the pixel threshold as described above, does need to be set carefully. If it is set too low, large portions of the time-frequency map can be identified as a single cluster. Therefore, we choose the value of  $\eta_{low}^{n,l}$  to ensure that all clusters are of reasonable size, which we define to be less than 50000 pixels. The value of  $\eta_{up}^{n,l}$  is chosen to be greater than this value, sufficiently large to avoid too many clusters being identified in the tuning runs, but sufficiently small to ensure that several clusters are identified for each box size. Theoretically, over many noise realisations the power in a specified pixel in the binned spectrogram should have mean  $\mu = 4$  and standard deviation  $\sigma^{n,l} = 2\sqrt{2/(n \times l)}$ , since it is the average of  $n \times l$  independent  $\chi_4^2$  samples. It would be reasonable to assign the minimal thresholds in the form  $\eta^{n,l} = \mu + \lambda \sigma^{n,l}$  for some constant  $\lambda$ . However, neighbouring pixels in the spectrogram are not independent as the binning boxes overlap.

Empirically we find that more suitable relations are

$$\alpha^{n,l} = 4 + \frac{10\sqrt{2}}{(nl)^{5/9}} \quad (3.2)$$

$$(\eta_{low}^{n,l})_{min} = 4 + 4\sqrt{\frac{10}{50000 + nl}} \quad (3.3)$$

$$(\eta_{up}^{n,l})_{min} = \max[\alpha^{n,l}, (\eta_{low}^{n,l})_{min}]. \quad (3.4)$$

The 5/9 exponent is slightly steeper than the theoretical value of 1/2, but the latter ignores the correlation between different pixels in the spectrogram. It is difficult to fully analyse the noise properties analytically due to the overlap between neighbouring boxes in the spectrogram. However, the 5/9 exponent was found to work well in simulations, providing enough clusters in each noise realisation to enable analysis, but not so many that each realisation took too long to analyse. Figure 3 illustrates the functions listed above, and the empirical data used to derive them. We note that for large box sizes, the curves cross and so we set  $\eta_{up}^{n,l} = \eta_{low}^{n,l}$ . Above this point, we no longer ensure that at least one cluster is found for each box size, as this is inconsistent with the more important requirement that no cluster exceeds 50000 pixels. We emphasise that our search is robust to the somewhat arbitrary choice of these minimal values.

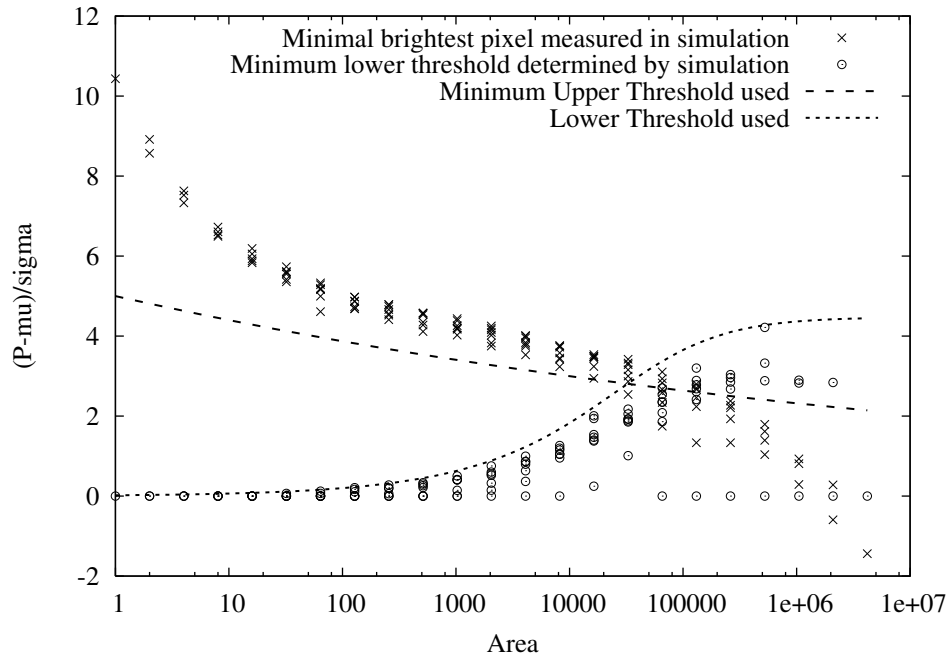


FIG. 3: Choice of the minimal threshold values employed in tuning HACR. The x-axis shows the box area,  $n \times l$  (note that generally there are several boxes with different shapes that have the same area). The y-axis shows the reduced threshold value,  $(\eta^{n,l} - \mu)/\sigma^{n,l}$ , where  $\mu$  and  $\sigma^{n,l}$  are the theoretical mean and variance of the power in a given pixel. Crosses indicate the smallest brightest pixel found in each box size over several hundred noise realisations, while circles indicate the smallest lower threshold that ensures no clusters greater than 50000 pixels over all noise realisations. The minimum upper threshold should lie comfortably below all the crosses to ensure at least one cluster is found in each realisation, while the lower threshold should lie above all the circles to ensure no  $> 50000$  pixel clusters are generated. Fits that satisfy these criteria are also shown, and are given analytically in the text. We note that for some of the largest box sizes, the reduced threshold,  $(\eta^{n,l} - \mu)/\sigma^{n,l} < 0$ . For the largest box sizes, there are only a handful of pixels in the binned spectrogram. There is thus a significant probability that the brightest of these will still be smaller than the mean in at least one realisation.

### C. Post-processing

For each box size we can consider values of  $\eta_{up}^{n,l}$  between  $(\eta_{up}^{n,l})_{min}$  and the maximum power measured  $(\eta_{up}^{n,l})_{max}$ , and construct a list of all clusters with peak power  $P_{max} > \eta_{up}^{n,l}$ , ordered by increasing number of pixels  $N_c$ . If the false

alarm probability in a given box size,  $AFAP$ , has been chosen, we expect to see  $M \times AFAP$  false alarms in  $M$  noise realisations. By looking at the list of clusters, we can identify a value of the threshold  $N_p^{n,l}$  with each value of  $\eta_{up}^{n,l}$  that would give the correct number of false alarms in the realisations considered. If HACR was run on pure noise with that pair of thresholds and only that one box size  $(n, l)$ , it would yield a detection rate  $AFAP$ . A typical relationship between  $\eta_{up}^{n,l}$  and  $N_p^{n,l}$  is shown in Figure 4. This was generated for a box size  $n = 1, l = 64$  for  $AFAP = 0.01, 0.005$  and  $0.0025$ .

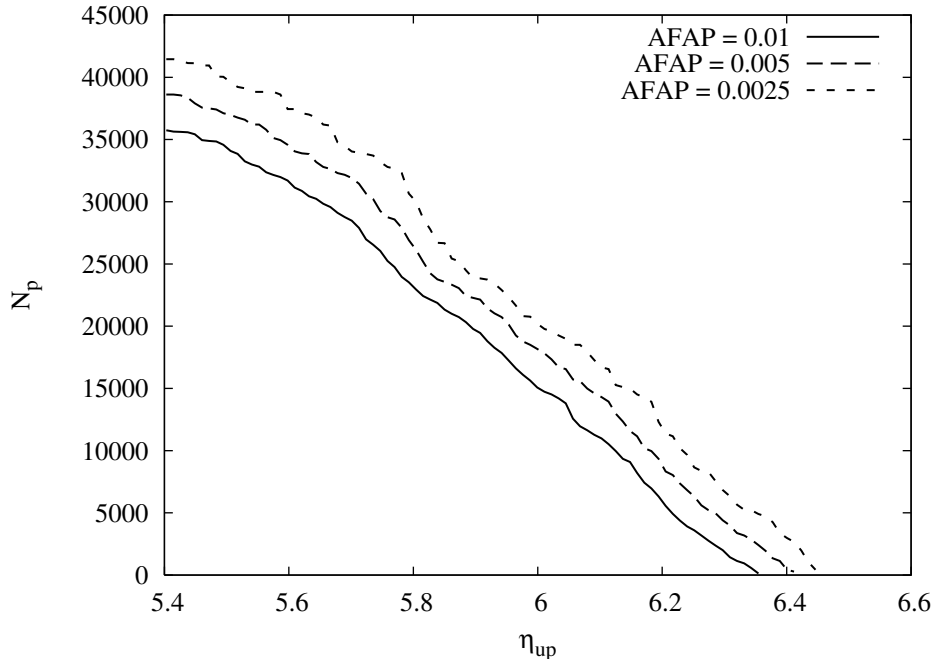


FIG. 4: Contours of constant (additional) false alarm probability shown for the box size  $n = 1, l = 64$ . Pairs of thresholds  $\eta_{up}$  and  $N_p$  which lie on a contour yield the same additional false alarm probability. It is intuitive that i) on a given contour a smaller value of one threshold corresponds to a larger value of the other threshold and ii) the contours spread out away from the origin for smaller false alarm probabilities.

To determine which combination of thresholds is optimal, we subsequently analyse spectrograms containing both noise and an injected signal. As mentioned earlier, since we are using white noise to generate the noise realisations, the signal is first whitened using the noise model described in Section II before injection. For each box size we may then select the pair of thresholds which yields the largest detection rate. Figure 5 shows detection rate plotted against threshold value for EMRI source “A” at a distance of 2Gpc using the box size  $n = 1, l = 64$  with  $AFAP = 0.01, 0.005$  and  $0.0025$ . Although only the  $\eta_{up}$  threshold value is shown a corresponding value of  $N_p$  is inferred. This stage of the analysis will be discussed further in the next section.

The full search uses multiple box sizes, searched in a particular order. We want the thresholds in a given box size to contribute an *additional* false alarm rate of  $AFAP$ , thus when determining the threshold combinations we need to ignore realisations in which false alarms have already been found. In practice, the procedure above is thus slightly modified when considering more than one box size. If we are using  $M$  noise realisations to determine the thresholds, each box size should give  $M \times AFAP$  false alarms. The necessary threshold combinations can be determined for the first box size as described above. It is then possible to identify the realisations in which the false alarms were found for the first box size. This set of realisations will be somewhat different for each of the pairs of thresholds that give the desired  $AFAP$ . So, in practice we must do this in conjunction with the source tuning described in the next section. This allows us to identify an *optimal threshold pair* and we can find the noise realisations in which *that* threshold pair gave false alarms. We then repeat the procedure described above, but now considering only the clusters identified in the remaining realisations. This is repeated for each box size in turn, ignoring in each subsequent box size any realisations in which false alarms have already been identified. This does mean that the order in which the different box sizes are searched is important. However, investigations suggest that it does not matter which order the box sizes are searched in, provided the order is the same for tuning and the actual search. This will be discussed further in Section IV A 1.

#### IV. PERFORMANCE OF HACR IN EMRI DETECTION

##### A. Tuning HACR for a single specific source

The fact that HACR has two thresholds allows the search to be tuned to optimally detect a specific source at a specific distance. For a given choice of false alarm probability,  $AFAP$ , we choose the combination of thresholds for each box size  $\eta_{low}^{n,l}, N_p^{n,l}$  that maximises the detection rate. For this optimal combination of thresholds, the detection rate can be computed for the given source and a Receiver Operator Characteristic (ROC) curve plotted for the HACR search tuned for that source. The ROC curve shows the detection rate as a function of the overall false alarm probability,  $OFAP$ , of the search using all box sizes.

In practice, the ROC is determined by generating a sequence of noise realisations, injecting the whitened signal into each one, and then constructing and searching the binned spectrograms. A detection is defined as any realisation in which a threshold pair is exceeded in at least one box size. The box sizes will be searched in the order they were constructed (see Figure 2). As for the false alarms discussed in the previous section, if a detection has been made for one box size, we want to ignore that realisation when we search with subsequent box sizes. This ensures that we always choose the threshold combination for a box size that provides the maximum number of *additional* detections. In practice, we achieve this goal by initially searching all the realisations using the first box size, for a number (typically  $\sim 100$ ) of pairs of thresholds that all yield the assigned  $AFAP$ . We then choose the threshold pair that yields the highest detection rate and identify every realisation in which *this optimal threshold pair* gave a detection. We then move onto the second box size and repeat this procedure, but only searching realisations in which the optimal threshold pair for the first box size did *not* yield any detections. As we proceed, the threshold combinations that yield the chosen  $AFAP$  for each box size are recomputed in light of the choices of optimal threshold, as discussed in the previous section. Note that as we do this, we are re-analysing two separate sets of noise realisations — one for characterizing the noise, and one in which the signal has been injected for characterizing the detection rate. Some care must be taken when determining what the detection rate is for the optimal threshold combination and in choosing the number of noise realisations to use in the various stages of this procedure. This is slightly technical and is relegated to A.

In Figure 6 we show the ROC curves for detection of source “A” at a range of distances. The random search line on this figure represents a search for which the detection rate and false alarm rate are equal. This is the “random

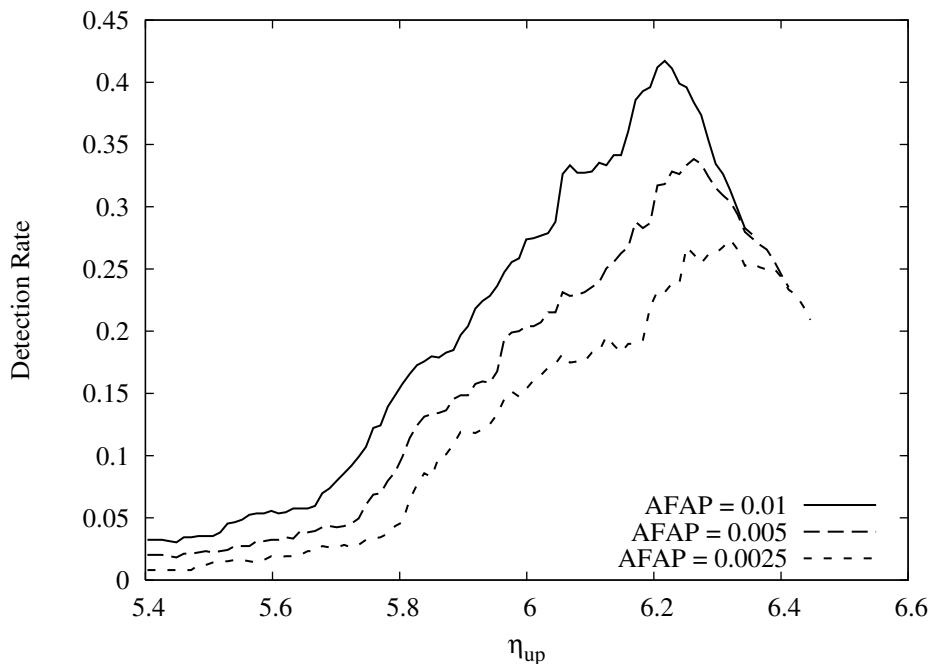


FIG. 5: Rate of signal detection plotted against choice of threshold. Each point on the x-axis represents a pair of thresholds which yield a particular value of  $AFAP$ . By choosing the threshold pair which yields the largest value of detection rate, plotted on the y-axis, we can maximise the rate of signal detection for a given false alarm probability.

limit” since it is equivalent to tossing a coin and saying that if it is heads the data stream contains a signal and if it is tails it does not. A search that yields a ROC curve equal to this random line is essentially insensitive to signals. In Figure 6, we see that the source has a 100% detection rate for all *OFAP*'s out to a distance of  $\sim 1.8$ Gpc. An overall false alarm probability of 10% is probably quite a conservative value, since this is the probability that *in a given LISA mission* the entire HACR search would yield just a single false alarm. Any value below 50% makes it unlikely that we would see any false alarms in the actual analysis. At a distance of 2Gpc, with the overall false alarm probability set to 10%, the detection rate is  $\sim 85\%$ . As the distance increases further, the detection rate further degrades, and the source becomes undetectable at a distance of  $\sim 3$ Gpc. The rate of EMRI events is somewhat uncertain, but the range for a  $10M_{\odot}$  black hole falling into a  $10^6M_{\odot}$  black hole is between  $10^{-7}$  and  $10^{-5}$  events per Milky Way equivalent galaxy per year [1, 2]. Using the same extrapolation as in [2], this gives  $0.1 - 10$  events  $\text{Gpc}^{-3} \text{ yr}^{-1}$ . Assuming a 3 year LISA mission, and that the detection rates quoted here are a good approximation to the fraction of EMRI events that LISA would detect in a single realisation of the mission, these rates translate to a detection of  $\sim 1.5-150$  events using this method (using a Euclidean volume-distance relation). We note, however, that at the high end of this range, source confusion will be a significant problem and it has been ignored in the current work.

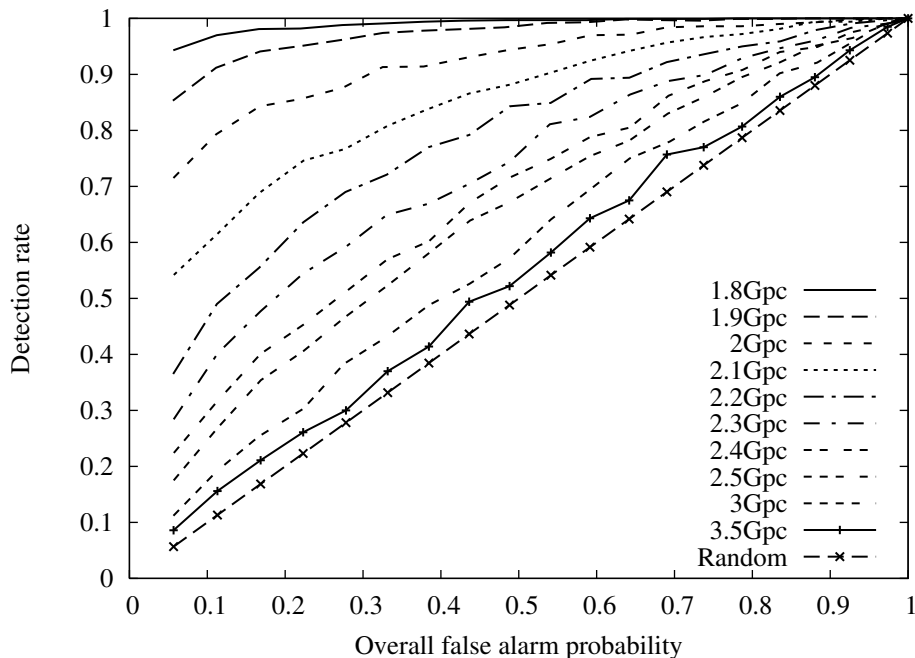


FIG. 6: Receiver operator characteristic (ROC) curves for detection of an EMRI (source “A”) at a range of distances from Earth. For each distance studied HACR was tuned in order to yield the maximum detection rate possible for every value of overall false alarm probability.

### 1. Comparing the performance of HACR and the Excess Power method

In Figure 7 we compare the performance of HACR and the Excess Power search by plotting ROC curves for both searches for detecting source “A” at a range of distances. Since HACR effectively performs the Excess Power search when  $N_p^{n,l} = 1$  we expect that HACR will always do at least as well as the Excess Power search. Due to the extra levels of tuning allowed by the HACR algorithm we find that it can obtain a slightly higher detection rate for a given false alarm probability. This is true when the source is at a distance of 2Gpc, but once the source is at 2.5Gpc, there is very little difference in the performance of the two searches. However, as illustrated in Figure 5, the optimal HACR pixel threshold tends to be significantly greater than 1. Thus, HACR identifies clusters containing significant numbers of pixels, while excess power at the first stage identifies only individual pixels. The information contained in the structure of the cluster should allow parameter estimation which can be used as input for later stages in a hierarchical search. Thus, although the event rate using HACR does not significantly exceed that of Excess Power, the information extracted from the time-frequency spectrogram is significantly larger in principle. Parameter extraction from the Excess Power method requires an additional track identification stage. Such algorithms are currently being

investigated [11], but HACR is more efficient, combining the two stages of source detection and cluster identification in a single algorithm. This will be discussed in more detail in Section VI.

As mentioned earlier, the fact that realisations in which detections are made are omitted for the search of subsequent box sizes treats the earlier box sizes preferentially. To ensure this does not bias the results, we must check that the overall search performance does not depend on the order in which the box sizes are searched. In Figure 8 we show ROC curves computed for the HACR and Excess Power searches, using the ordered search, and three randomized search orders. There is a small amount of scatter in these results which can be attributed to randomisation in the noise, but it is quite clear that the overall performance is independent of the box size search order. We recommend using the order given by the efficient binning algorithm described earlier because of the computational savings.

In Figure 9 we show how the detection rate depends on the box size. This figure shows the number of detections made for each box size over the 1000 realisations used for determination of the ROC curve for source “A” at 2Gpc. It is clear that there is not one single box size that makes all the detections, but several box sizes are important. This is because random noise fluctuations will sometimes make one box size better than another. However, it is also clear that many of the box sizes do not make any detections and are apparently not very useful for the detection of this particular source. This is partially due to the box size search order. Figure 9 also shows the detection rate as a function of the box size label when the search order was randomized. Although the distribution is qualitatively the same, the box sizes that make the detections are different in this case. The reason for this is clarified by Figure 10 which shows the same detection rates, but now as a function of the order in which the box sizes are searched. It is clear that there are several box sizes that are equally good at detecting this source (these have approximately the same dimension in frequency, but different dimensions in time). Whichever of these equivalent box sizes is used first will make the detection, although the overall number of detections and ROC performance is independent of the search order. The fact that there are some box sizes that are efficient at detection of source “A”, but others that are not, suggests that the search performance might be improved by using only a few box sizes. This will be discussed in the next section.

## B. Targeted searches

We have seen in Figure 9 that the majority of detections of simulated signals are made by only a handful of box sizes. As discussed earlier, there are certain box shapes which are likely to be efficient at detecting certain types of

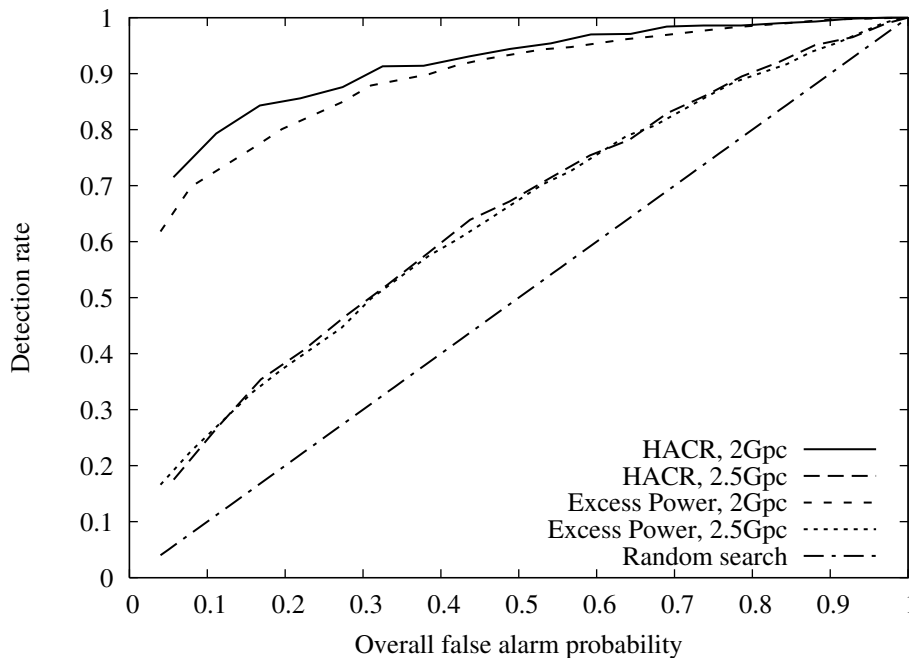


FIG. 7: Receiver operator characteristic (ROC) curves for detection of an EMRI (source “A”) at a range of distances from Earth. For each distance we compare the ROC obtained having tuned HACR for that distance to the ROC obtained using the Excess Power search. As expected HACR’s performance either matches or exceeds that of the Excess Power search.

signal. In the case of source “A”, we find that boxes which are moderately broad in frequency, but fairly narrow in time, are good for detection, e.g., the best box size in the ordered search had dimension  $1 \times 128$  in time  $\times$  frequency. Boxes that were very large in frequency and time, e.g.,  $32 \times 65536$ , did very poorly at detecting source “A”. The box

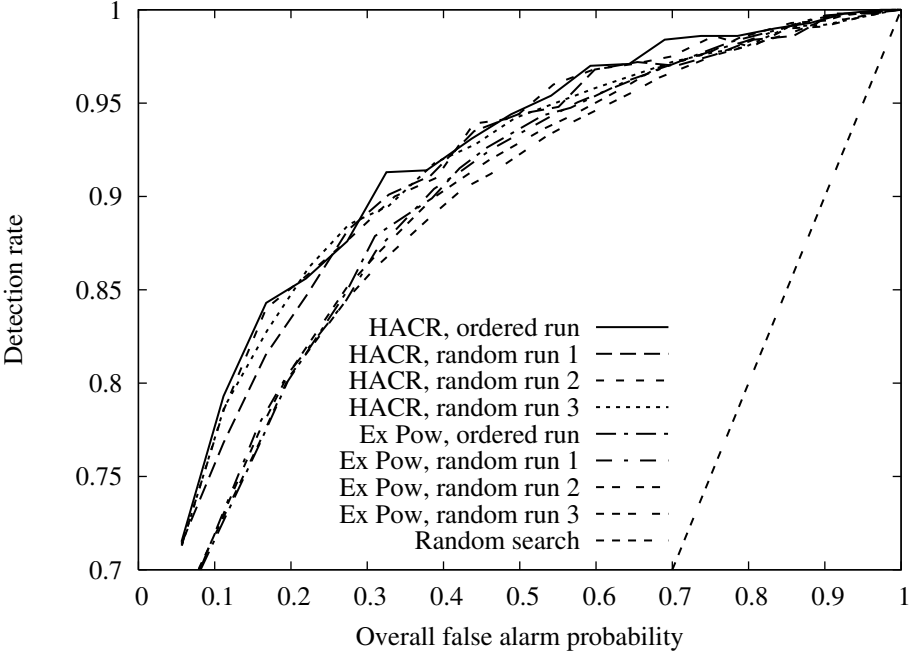


FIG. 8: ROC curves for detection of source “A” at a distance of 2Gpc using HACR and Excess Power when the search order is randomized.

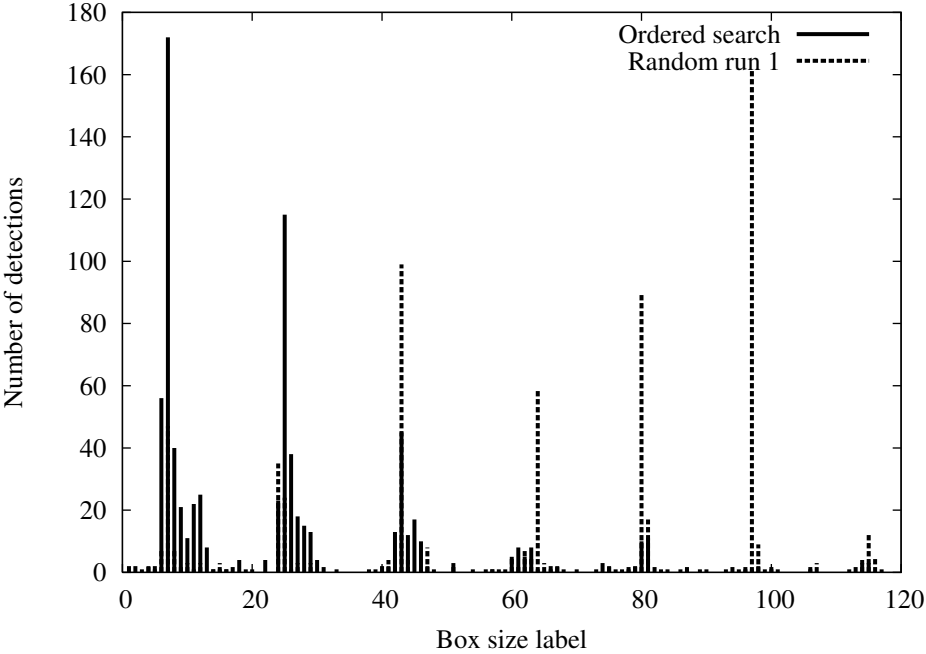


FIG. 9: Number of detections as a function of box size when searching 1000 realisations of source “A” at 2Gpc. Results are shown when using the ordered search, and when the box size search order is randomized. The x-axis is the box size label, which corresponds to the order in which the boxes are analysed in the *ordered* search.

sizes in which detections are made reflect the structure of the GW signal and are a diagnostic of the physical properties of the source. However, there will be multiple box sizes that are good for a given source, e.g., an instantaneously monochromatic source whose frequency evolves slowly in time will be detected in boxes that are narrow in frequency and long in time. However, boxes of time dimension  $l$ ,  $2l$  and  $4l$  may all be well suited to its detection. The presence of noise may occasionally wash out the signal in one of these box sizes, but not necessarily in the others. Thus, although not all box sizes are suited for detection of a particular source, more than one will in general be required to maximize the detection rate in the presence of noise fluctuations. This is why there are multiple peaks in Figure 9.

Given that we have specified thresholds so that each box size contributes equally to the overall false alarm probability we might expect the search to perform better if we restrict it to use only those few box sizes responsible for most of the detections of the injected signal. By eliminating box sizes that make few detections, we expect to reduce the overall false alarm probability while keeping the overall detection rate approximately constant, thereby improving the overall ROC performance.

The effect of targeting the search to a restricted number of box sizes can be investigated by re-analysing the data using only the 10 box sizes, out of the 119 box sizes considered, that were responsible for the most detections of EMRI source “A”. As we saw earlier, the order in which the box sizes are searched affects the number of detections made and therefore the 10 “best” box sizes are not uniquely determined. We used the results from the full ordered (rather than randomized) search of all 119 box sizes to choose the 10 best box sizes which were then analysed again (in the same order) in the targeted search. Having performed the search using only 10 box sizes, we eliminated the box size which had the worst performance (i.e., the least number of detections) *in the 10 box search* and then repeated the search with the remaining 9 box sizes. This process was repeated, eliminating one box size each time, until only one box size remained. The box size that contributes the fewest detections depends to a limited extent on the (additional) false alarm probability assigned to each box size. We used the additional false alarm probability that gave an overall search false alarm probability of  $\sim 10\%$  since, as argued earlier, this would be a reasonable value to use in the final LISA search.

In Figure 11, we show ROC curves for the targeted search when source “A” is injected at a distance of 2Gpc. For comparison, we also include ROC curves for the full search, and for the full Excess Power search. The Excess Power results were constructed from our data by fixing the pixel threshold,  $N_p = 1$ , as described earlier. We also computed ROC curves for the targeted Excess Power search, but in most cases the performance was the same as for HACR with the same number of box sizes. The exception was the Excess Power search using only 1 box size which performed noticeably worse than HACR with only 1 box size, and the corresponding ROC curve is shown. It is clear from the Figure 11 that the targeted HACR search follows our intuition to some extent. When the number of box sizes is

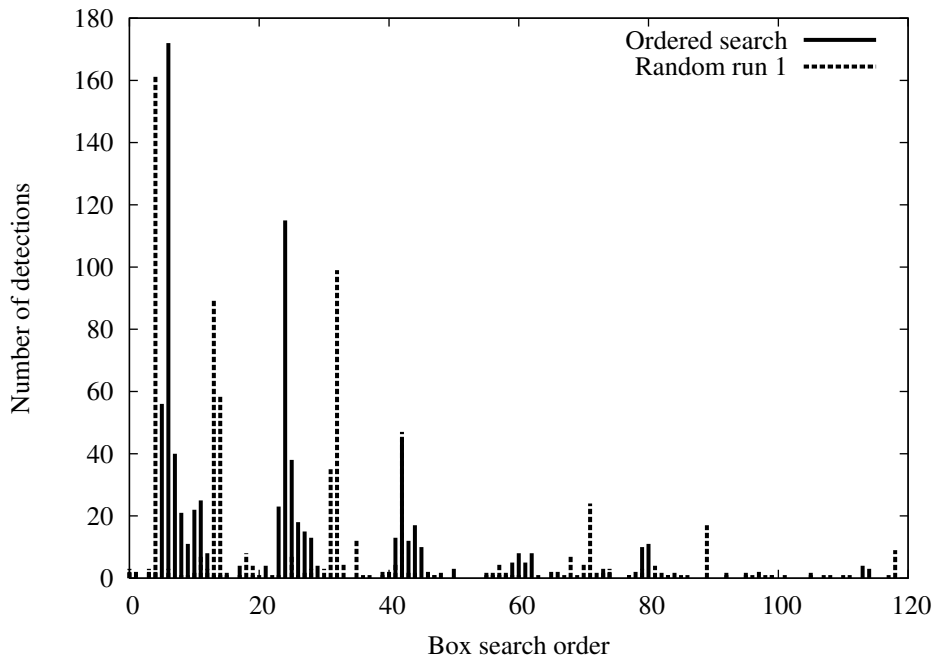


FIG. 10: As Figure 9, but now the x-axis is the order in which the boxes were analysed in each particular search.

reduced from 119 to 10, the ROC performance does improve as the overall FAP reduces, while the detection rate remains largely unchanged. However, this improvement is not particularly marked. As the number of box sizes used is reduced further, the ROC performance remains roughly constant until only 4 box sizes are being used. The ROC performance in that case is quite comparable to the full search. Using fewer than 4 box sizes leads to performance that degrades and is always worse than the full search. This is in keeping with the understanding that several box sizes are needed for efficient detection of a source due to the effect of noise fluctuations.

The performance of the search was also examined using a larger number of box sizes, but it was not possible to do better than the 20 box size search, which is also shown in Figure 11. The possible effect of randomisation was also explored by taking the ten best box sizes from a random search and following the procedure described above to eliminate box sizes successively. The search order was randomized again after each box size was removed. These calculations gave the same results as those shown in the figure.

We conclude that it is possible to improve the performance of the search for a specific source by targeting to fewer box sizes. However, the improvement is not that significant. This is consistent with what was found for the Excess Power search [10]. Since the box sizes that are efficient for the detection of one particular source will almost certainly not be the same as those that are efficient for other sources, the best approach is to include all the box sizes in the search. However, since there are certain box shapes that are good for detecting certain types of source, the box size for which a given detection is made provides a diagnostic of the source system.

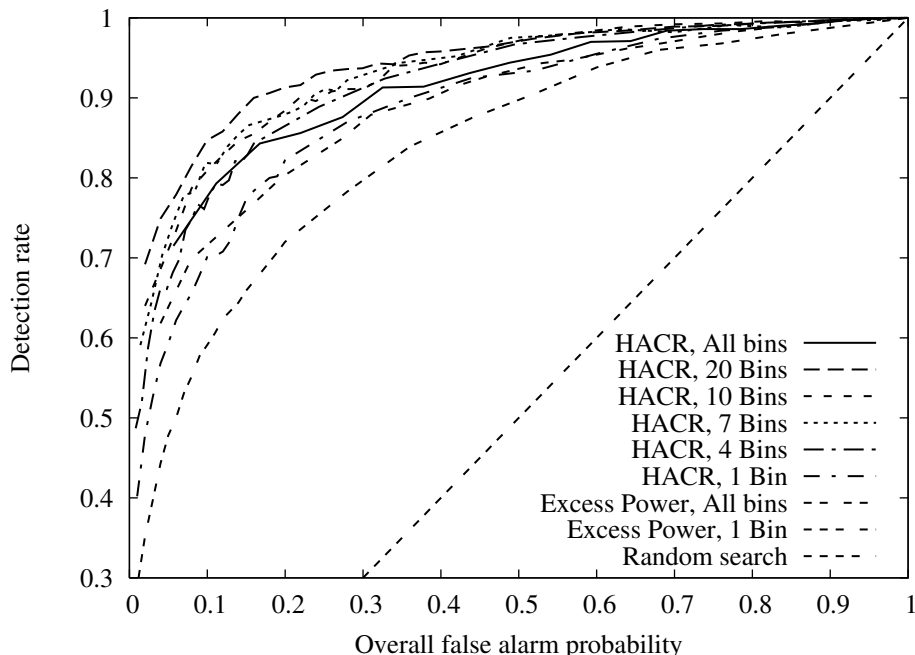


FIG. 11: ROC curve for targeted HACR and Excess Power searches with source “A” injected at a distance of 2Gpc. The figure shows the detection rate (y-axis) as a function of the overall search false alarm probability (x-axis) for the HACR and Excess Power searches when the number of box sizes searched is restricted as described in the text. The number of box sizes used for each curve is given in the key.

### C. Detection of other EMRI sources

The results described in the preceding sections have focused on the detection of one particular EMRI, source “A”. We have also explored the usefulness of HACR in the detection of other EMRI events. To do this, we selected some of the EMRI sources used for the investigation of the Excess Power search [10]. Specifically we used the sources “K” and “N”, which have the same parameters as source “A” except for eccentricity. The source “K” is circular at the start, while source “N” has eccentricity of 0.7, compared to  $e = 0.4$  for source “A”. We placed these sources at a range of distances between 1.5Gpc and 2.7Gpc, and injected them into noise realisations. We were thus able to determine ROC curves for detection of these sources via the method detailed in A. In Figure 12 we compare the ROC curves for detection of these sources with HACR when they are at a distance of 2Gpc. We see that our ability to detect a system

at a given distance is better for binaries in circular orbits (source “K”) than for systems with eccentric orbits (sources “A” and “N”). This is consistent with what was found for the Excess Power search in [10]. The predominant effect of orbital eccentricity is to split the GW radiation power into multiple harmonics. As the eccentricity increases, the frequencies of these harmonics become increasingly separated. As a consequence, a given box in the time-frequency map contains a smaller ratio of signal power to noise power. The detectability of EMRI sources therefore decreases as the eccentricity is increased.

The performance of the HACR search for other sources considered in [10] is similar in general. The overall detectability follows the same pattern as the Excess Power search. HACR has a slightly greater detection rate than Excess Power when the source is nearby, but as the source is put further away, the performance of HACR and Excess Power become comparable before the random limit is reached. However, in all cases, the HACR detection is made with a lower upper threshold than Excess Power, compensated by a larger pixel threshold. Thus, HACR detections identify clusters with significant numbers of pixels, the properties of which will be invaluable for subsequent parameter estimation. This will be discussed in Section VI and will also be the subject of a follow-up paper that is currently in preparation.

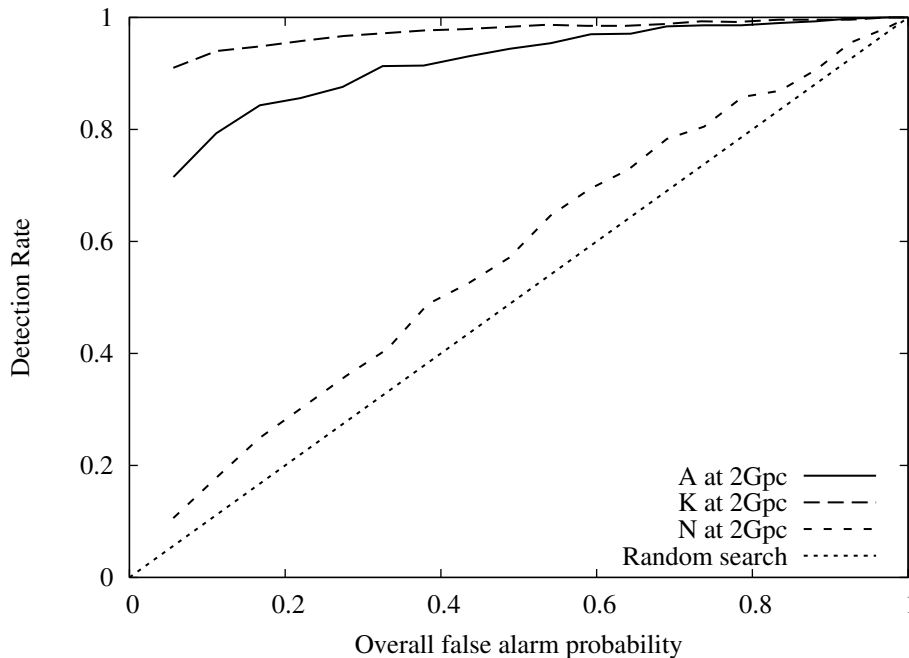


FIG. 12: ROC curves for detection of EMRI sources “A”, “K” and “N” at a distance of 2Gpc using HACR.

#### D. Tuning HACR for multiple sources

In the preceding sections, we have focused on detection of a single source at a fixed distance. However, in the actual analysis of LISA data, we will not know a priori what sources will be in the data stream, and so the HACR thresholds need to be tuned as generally as possible. Even in the case of a single EMRI source, the optimal threshold pair depends to some extent on the distance at which the source is placed. This is in contrast to the Excess Power search, where there is only one threshold that is uniquely determined by the choice of false alarm probability. There are two possible approaches to constructing a general HACR search — 1) have several separate HACR searches, targeting different sources and using different sets of thresholds or 2) have a single HACR search with a set of thresholds chosen to be sensitive to as many LISA sources as possible. To date, we have focussed on the latter approach, since our results have shown that it is possible to do almost as well with a single set of “generic” thresholds as with source specific thresholds.

As a first step, we took the thresholds designed to optimally detect source “A” at 2Gpc and used those thresholds to search for sources “K” and “N”. The results are shown in Figure 13. We see that there is some degradation of performance, but this degradation is very small. This is a promising result and suggests that certain threshold combinations do well at detecting all the EMRI events.

It is also possible to tune the thresholds to be generally sensitive to many different sources. It is clear from Figure 13 that this is not really necessary for the case of EMRI detection, but we will describe the procedure here as it will be needed when other types of source are included in the search. The most logical way to tune the search is so that the total LISA event rate (i.e., number of events observed) is maximized. If we knew in advance which sources would be present in the LISA data, we would tune the search by considering multiple noise realisations with that family of sources injected and choosing the threshold combination that gives the maximum total detection rate for given assigned FAP. Since we do not know what the actual sources in the LISA data will be, we can instead tune the thresholds to be as sensitive as possible to a *single* event of unknown type, using prior knowledge to weight the relative likelihood of different types of event. This procedure ignores issues of source confusion, but should ensure that the loudest events are detected, no matter of what type or at what distance they might be.

In practice, the tuning for multiple sources is done in a similar way to the single source tuning described earlier. First, combinations of thresholds that give a specified *AFAP* are identified using analysis of pure noise realisations. Then, a set of realisations of noise plus injected signal are generated for each of the possible signals that we wish to tune for. For each of  $\sim 100$  threshold pairs that yield this *AFAP* in each box size, the HACR search is performed for each set of signal injections, and the rate of detections for each source,  $R_s$ , is determined. This is all the same as the tuning procedure for a single source. However, we then add the detection rates for all the source types together, multiplying by weighting factors  $w_s$  chosen to reflect our prior understanding of the relative likelihood of that particular source. We then choose the threshold pair that maximizes the sum  $R_s \times w_s$  over all the source types considered. As in the single source case, box sizes are considered sequentially, and all realisations in which detections for a given source type are made for the optimal threshold pair are ignored for the analysis of that source type in subsequent box sizes. Once this procedure is complete, new sets of signal injections can be analysed using these optimal thresholds to determine the final ROC curve.

One remaining question is what to use for the weighting factors. If we knew that only one type of source existed in the Universe, but it was equally likely to be at any point in space, we would use a volume weighted average. We do this by taking our set of sources to be a single given source placed at a sequence of distances,  $d_i$ . The source at distance  $d_i$  can then be regarded to be representative of all sources in the range  $d_{i-1} < d < d_i$ , and should be weighted by the (Euclidean) volume of space in that range,  $w_i \propto 4\pi(d_i^3 - d_{i-1}^3)/3$ . This is illustrated schematically in Figure 14. We carried out this procedure using source A at distances of 1.5Gpc, 1.6Gpc, ..., 2.7Gpc, with weightings 1,  $(1.6/1.5)^3 - 1 = 0.214$ ,  $(1.7/1.5)^3 - (1.6/1.5)^3 = 0.242$ , ...,  $(2.7/1.5)^3 - (2.6/1.5)^3 = 0.624$ . Note that we have calculated the weighting factors relative to the factor for the volume  $d < 1.5$ Gpc. We took the closest source to

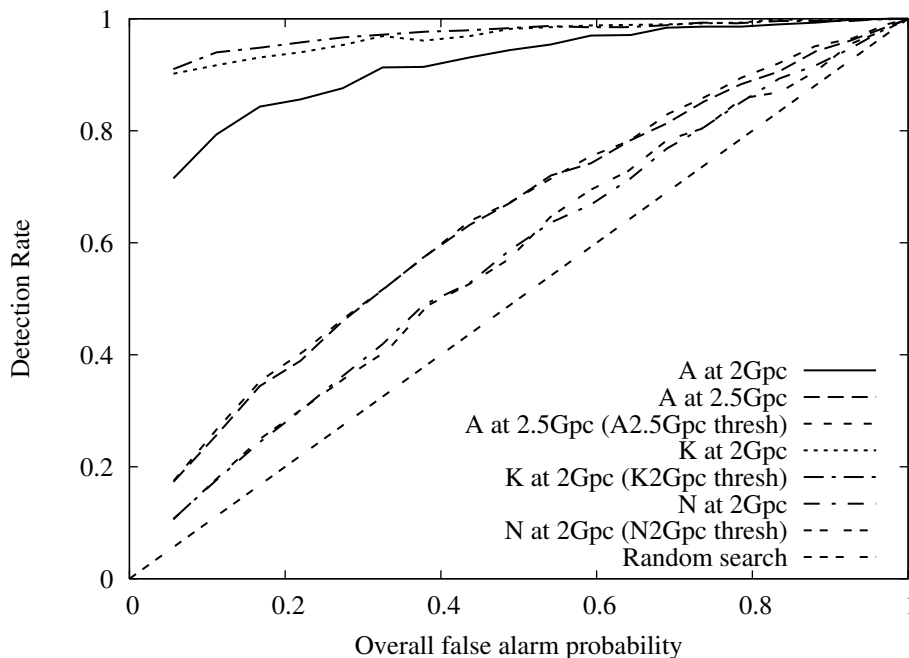


FIG. 13: ROC curve for detection of sources “A”, “K” and “N” at various distances, using thresholds chosen to maximize the detection rate of source “A” at 2Gpc. For comparison, the ROC curve for detection of each source with thresholds tuned for that source is also shown in each case, e.g. the curve denoted as “K at 2Gpc (K thresh)”.

be at 1.5Gpc since up to that distance, the detection rate is always 100%. This appears to give artificial weight to the 1.5Gpc source, but in practice this does not happen since virtually every threshold pair gives a 100% detection rate for that source, and the variation in rate is determined primarily by the other injections. We used the distance weighted thresholds determined in this way to search for source “A” at various distances. The resulting ROC curves are shown in Figure 15. Although the thresholds do change to some extent as a result of this tuning procedure, these changes are small since the optimal thresholds are almost independent of distance, and so we find that the overall ROC performance is largely unaffected. We deduce that it is possible to detect a given EMRI source at any distance with a single set of thresholds.

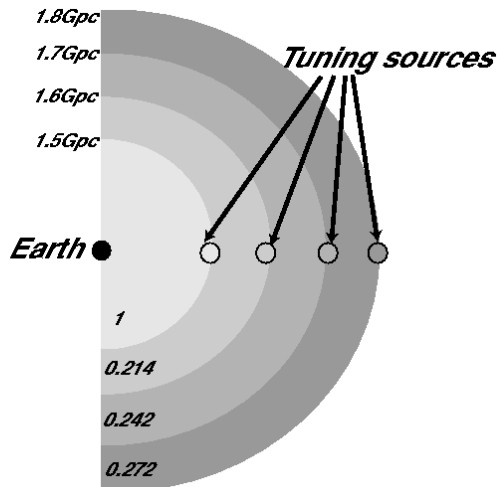


FIG. 14: Illustration of procedure to compute distance averaged thresholds. We consider a source placed at a sequence of distances,  $d_i$ , regarding each one to represent that source at any distance closer than  $d_i$ , but further than  $d_{i-1}$ . Volumes are shaded according to the source chosen to represent them. Note that the weighting factors are quoted relative to the weighting factor for the volume  $d < 1.5\text{Gpc}$ .

LISA will not only see one type of source, but we can fold in prior information about the relative abundance of different events by adjusting the weighting factors. As an illustration, we followed this procedure to tune for sources “A”, “K” and “N” all placed at a single distance of 2Gpc, and given equal weighting. In that case too, we found that the ROC performance was not significantly changed when tuning for these multiple sources. As a final example, we also tuned for all three sources, placed at all the distances, 1.5Gpc, ..., 2.7Gpc, with the volume weightings listed previously. Once again, the ROC performance was not significantly altered. Thus, there is a single set of HACR thresholds that can detect all three EMRI sources at any distance.

These results may not be truly generic, since the three EMRI sources are quite similar, differing only in eccentricity. It is therefore perhaps unsurprising that a single set of thresholds can detect all three sources almost optimally. However, we saw in Section IV B that it is only a handful of box sizes that make a significant fraction of the detections of a given source. If we are tuning for sources that have very different time-frequency characteristics, the chances are that the box sizes needed for each will be different, so the tuned search will essentially use one set of boxes for detection of one particular type of source and another set of boxes for detection of a different type of source. Moreover, we know that HACR includes the Excess Power search as the pixel threshold  $N_p = 1$  limit. The Excess Power search thresholds are independent of the tuning source at fixed assigned FAP. Thus, a HACR search tuned for a collection of sources can do no worse than the Excess Power search for each of those sources. Since the HACR search does not seem to hugely outperform the Excess Power search, we would not anticipate that this combined tuning procedure would lead to a serious degradation of performance even when considering very different classes of source.

## V. PERFORMANCE OF HACR IN DETECTION OF OTHER SOURCES

We have shown that HACR may successfully be tuned in order to detect multiple EMRI sources with different parameters. In this section we investigate HACR’s ability to detect other classes of signals, specifically those emitted by white dwarf (WD) binaries and by the merger of supermassive black hole (SMBH) binaries. We expect these other classes of signal to have quite different structure in a time-frequency map. A typical EMRI signal consists

of several frequency components (due to the eccentricity of the orbit), which “chirp” slowly over the course of the observation, i.e., the frequency and amplitude increase. By contrast, the GW emission from a WD binary is essentially monochromatic. A SMBH binary inspiral also gives a chirping signal, but the chirp occurs much more quickly than the EMRI due to the increased mass ratio, so it will be characterised by a signal that is broader in frequency. This difference in structure allows HACR to be tuned for all three types of source simultaneously.

### A. A typical SMBH binary source

As a preliminary investigation of the ability of HACR to detect other classes of source, we followed the tuning procedure described earlier, injecting a typical SMBH binary inspiral and a typical WD binary at various distances. The SMBH binary waveform represented the inspiral of two  $10^6 M_\odot$  non-spinning black holes, placed at a random sky position, and with merger occurring  $\sim 3$  weeks before the end of the observation. The masses are the intrinsic masses of the black holes, i.e., not redshifted. When the source was placed at higher redshift there are therefore two effects — an increase in the luminosity distance to the source, and a redshifting effect — which pushes the signal into the less sensitive part of the LISA noise curve. In Figure 16 we show the ROC curves for detection of this SMBH binary source at a range of redshifts. At each redshift the optimal thresholds were chosen using the tuning method described in Section IV A. We find that SMBH binary sources at redshifts  $z \leq 3$  are detected with almost perfect efficiency using HACR, but we stop being able to resolve signals for redshifts  $z > 3.5$ . This is primarily because the (matched filtering) SNR of the source decreases significantly due to the redshifting effect mentioned above.

### B. A typical WD binary source

The “typical” WD binary was chosen to have the parameters of RXJ0806.3+1527 (as quoted in [22]), except for distance and sky position. The latter was chosen randomly, but this choice, and the noise model used meant the SNR of this source at a distance of 1kpc was approximately a factor of 3 greater than that quoted in [22]. This should be born in mind when considering the distances quoted in the following discussion. In Figure 17 we show the ROC curve for this WD source, injected at various distances. At distances  $\leq 15$ kpc, we obtain near perfect detection using HACR.

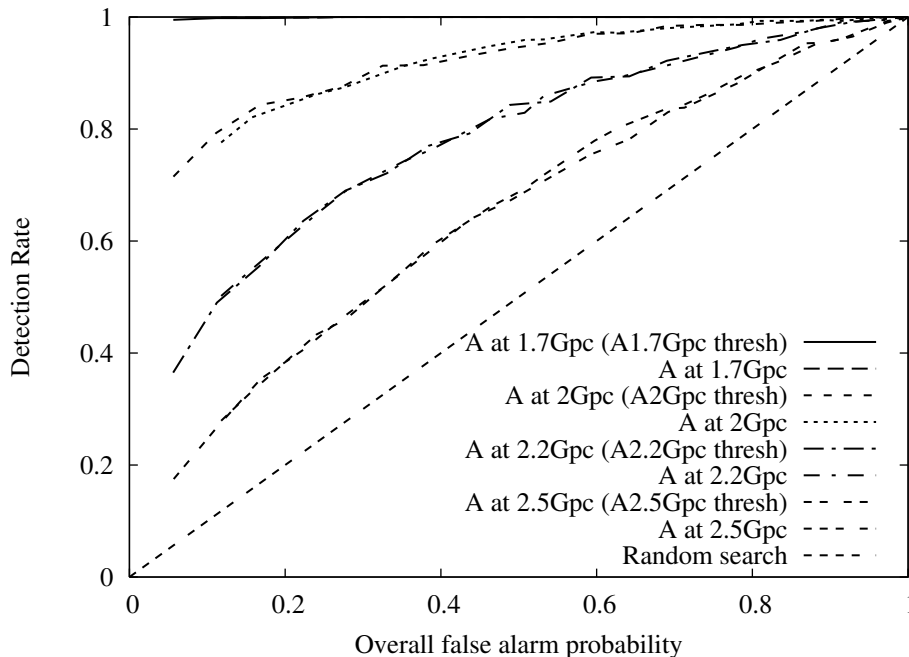


FIG. 15: ROC curves for detection of source “A” at various distances, when the thresholds are determined by the volume weighted average described in the text. For comparison, the optimal ROC curves for each distance (using thresholds tuned for that particular distance) are also shown, e.g. “A at 2.2Gpc (A2.2Gpc thresh)”.

The sensitivity falls off rapidly for greater distances and the source becomes undetectable at greater than  $\sim 20$ kpc. Even allowing for the SNR discrepancy mentioned above, this source would be detectable at  $\sim 6$ – $7$ kpc, so almost at the distance of the galactic center. Since this particular source is estimated to be at a distance of  $300$ – $1000$ pc, it would be detectable via this method. We would expect to detect other white dwarfs at distances of  $1$ – $10$ kpc depending on the source parameters. This does not allow for source confusion, as we have only injected single sources into the data stream, but the conclusion for RXJ0806 should be robust, since it radiates at  $\sim 6$ mHz, which is in the regime where WD binaries are well separated in frequency.

In the preceding plots, we have tuned HACR thresholds to detect the source in question, at a particular distance. If instead we imagined that we would use only one set of thresholds, tuned for EMRI source “A” at a distance of  $2$ Gpc, then the ROC performance for detection of the SMBH binary and WD binary events is significantly degraded. This is shown in Figure 18, which compares the ROC curve for detection of the SMBH binary at redshift  $z = 3.125$  and the WD binary at a distance of  $17$ kpc when the EMRI thresholds are used, versus the result when the source specific tuned thresholds are used. We see that using the EMRI thresholds typically reduces the detection rate by a factor of 5 or more.

### C. Tuning HACR for multiple classes of source

One solution to this problem in a LISA search would be to run several independent searches focussed on different source families. However, it is also possible to tune a single set of HACR thresholds to be sensitive to all three types of source simultaneously. This is done in the same way as the source and distance-averaged tuning described in Section IV D, but now we inject both EMRI, WD and SMBH events. When the thresholds are tuned using EMRI source “A” at  $2$ Gpc, the WD binary at  $17$ kpc and the SMBH binary at  $z = 3.125$  with equal weighting, the ROC curve for detection is as shown in Figure 19. We only show ROC curves for the EMRI and WD binary sources to avoid confusion on the plot, but the conclusions for the SMBH binary are the same. It is clear from this figure that when the sources are tuned for all three types of source, the performance of HACR is virtually restored to the optimal level, and still exceeds the performance of the Excess Power search. That this is possible follows from the different time-frequency properties of a source determine which box sizes are good for its detection. This is illustrated in Figure 20, which shows schematically all box sizes that contribute more than 1% of the detection rate for four different types of source: EMRIs “A” and “K”, the WD binary

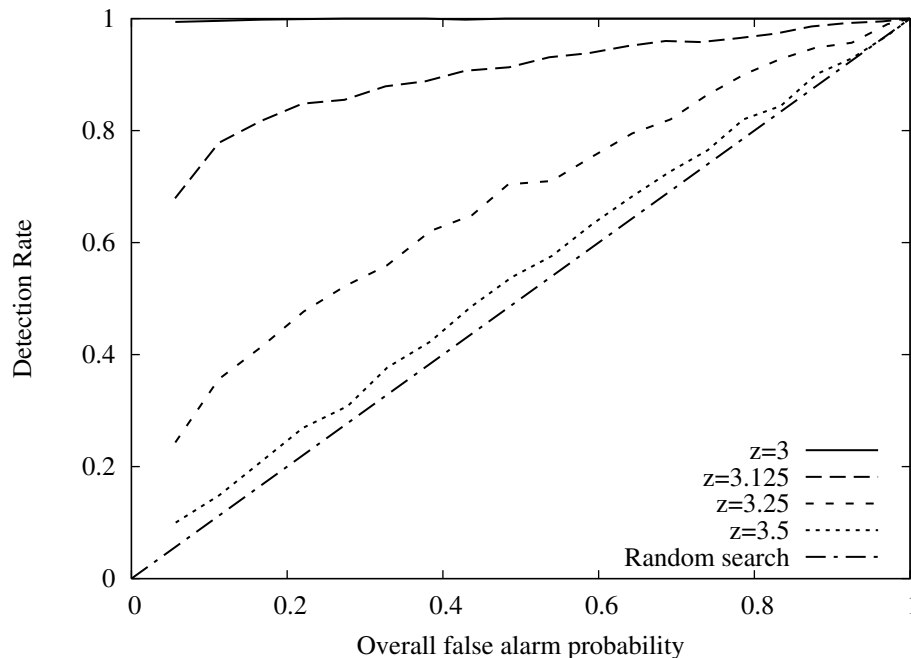


FIG. 16: ROC curves for detection of a SMBH binary at various distances. The optimal thresholds for each distance were chosen using the tuning method described in section IV A

and the SMBH binary inspiral. Physically, we expect WD binary tracks to be virtually monochromatic, and of long duration. Therefore we might expect to detect such sources in box sizes that are long in time but very narrow in frequency. The SMBH binary inspiral (at that redshift) is fairly short in duration, but sweeps through a reasonable range in frequency and is also quite loud. Therefore, we might expect to see it in boxes that are narrow in time, and

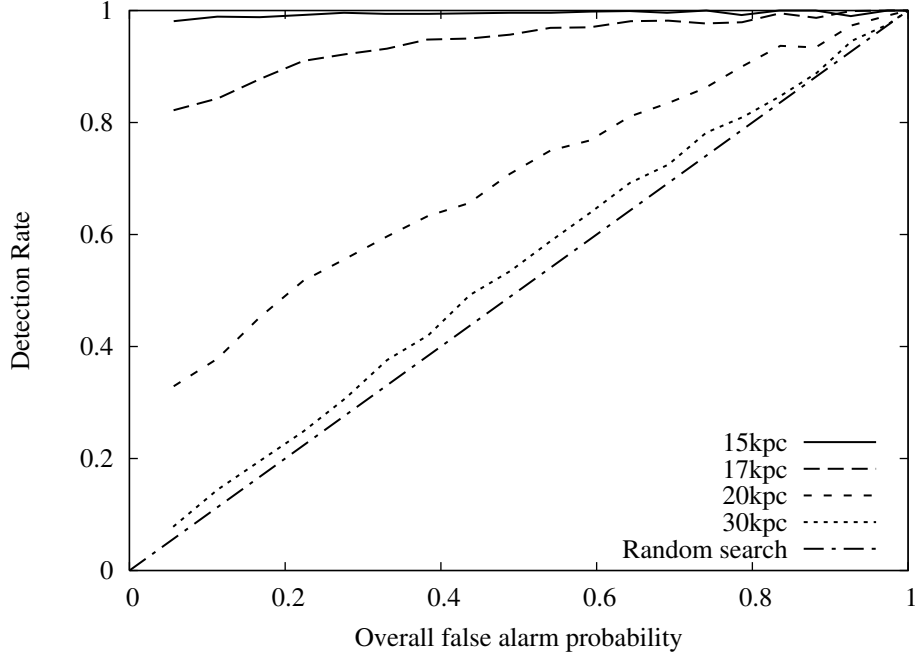


FIG. 17: ROC curves for detection of a WD binary at various distances. The optimal thresholds for each distance were chosen using the tuning method described in section IV A

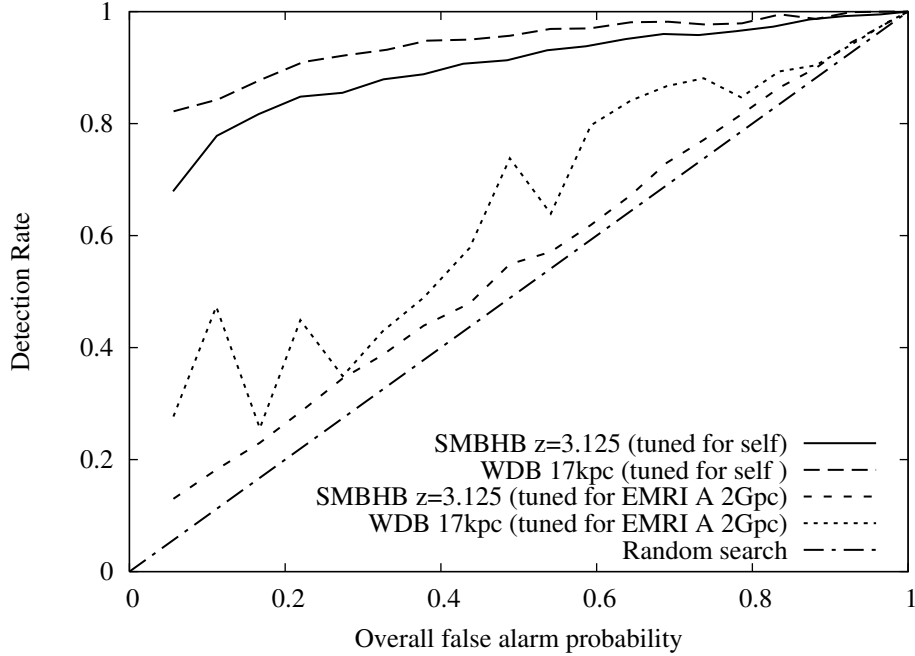


FIG. 18: ROC curves for detection of the SMBH and WD binary sources using thresholds tuned for EMRI source "A" at a distance of 2Gpc. For comparison, the ROC performance when the search is tuned for the source in question is also shown.

broader in frequency. EMRIs are similar in structure to SMBH binary inspirals, but last longer in time and evolve more slowly. For a circular EMRI (e.g., source “K”), one might expect to detect it in boxes that were long in time and quite narrow in frequency, although shorter in time and slightly broader in frequency than the WD binary (since the frequency narrow changes as the source inspirals). However, an eccentric EMRI (e.g., source “A”) will have multiple frequency harmonics, and one might expect to do better using a slightly broader box in frequency which then includes more of the frequency components. The distribution in Figure 20 fits precisely with this physical intuition. When tuning for multiple sources, the threshold in a given box size will be determined by the source that the box size is most suited to detecting. The fact that the various types of source favour distinct groups of box sizes means the overall performance is comparable to the source specific performance. The box sizes in which HACR detections are made provide an additional way to classify the source type.

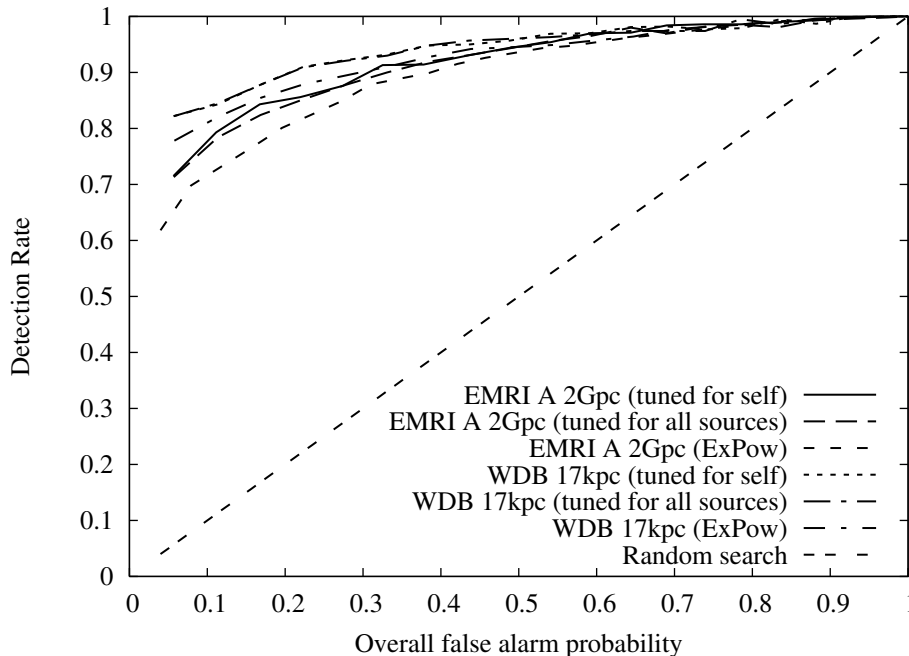


FIG. 19: Comparison of ROC performance for detection of EMRI source “A” at 2Gpc and the WD binary at 17kpc using i) thresholds tuned for that particular source; ii) the Excess Power search; iii) thresholds tuned for all three types of source.

## VI. USING HACR FOR PARAMETER ESTIMATION

We have emphasised throughout this paper that, although the HACR search does not provide a much greater detection rate than the Excess Power search, the clusters it identifies may be used to characterize the source. An Excess Power detection essentially contains two pieces of information — the time and frequency at which the detection is made. Since we are using binning as part of the search, there is also some information contained in the box size(s) used to bin the spectrogram(s) in which the detection(s) is (are) made. To gain further information, a detection made by Excess Power must be followed by a track identification stage, and this is currently being investigated [11]. A HACR cluster by contrast consists not of one but many pixels. Thus, in addition to the previous properties, the HACR cluster has shape information which is a much more powerful diagnostic. The information that can be extracted ranges from the simple size of the event in time and frequency to the more complicated shape and curvature of the boundary of the cluster. An event that is short in the time direction but broad in frequency might be an instrumental noise burst, whereas events long in time and narrow in frequency are probably inspiral events. The difference in frequency between the latest and earliest pixels in the cluster, divided by the difference in time, provides an estimate of the rate of change of frequency (or chirp rate) of the event. The shape parameters [23] of the cluster also provide diagnostics which might be able to distinguish instrumental bursts from astrophysical bursts from long lived astrophysical events. As mentioned elsewhere, source confusion is a major issue for LISA, with many events likely to be overlapping in time and frequency in the data stream. A detection in the time-frequency plane could therefore either be a single source

or several overlapping sources. An analysis of the cluster boundary should be able to distinguish these two cases in certain situations, i.e., distinguish a “cross” from a “line”.

The power profile in the cluster is also a potentially useful diagnostic. One use would be to distinguish crossing tracks from inspirals as above. Additionally, the power profile along an inspiral track would reveal the modulations associated with the motion of the detector and thus provide a diagnostic of sky position. In a more sophisticated analysis, cluster properties would allow different clusters that are generated by the same event to be identified. An EMRI is characterized by several different frequency components and these might well appear as different clusters in a time-frequency analysis (see spectrograms in [9]). However, these tracks remain almost parallel as they evolve, and so the rate of change of frequency provides a way to connect the tracks in a second stage analysis of the HACR clusters. If tracks can be identified like this, the properties, such as the track separation, encode information about the orbital eccentricity etc.

One complication in all of this is that the construction of the binned spectrograms makes use of bins that overlap in time and frequency. This has the effect of smearing out tracks from astrophysical sources and noise events in the data, which complicates cluster characterisation and parameter extraction. In analysing cluster properties, this effect must be accounted for, or methods derived to deconvolve the effect of binning once a source has been identified.

It is clear that HACR cluster properties are a potentially powerful tool both for vetoing, i.e., distinguishing astrophysical events from instrumental artefacts, and for parameter estimation. Work is currently underway to investigate which of these and other cluster properties are most powerful as diagnostics, and how the system’s parameters may be estimated from them. However, we leave a fuller discussion of this analysis and the results for a future paper.

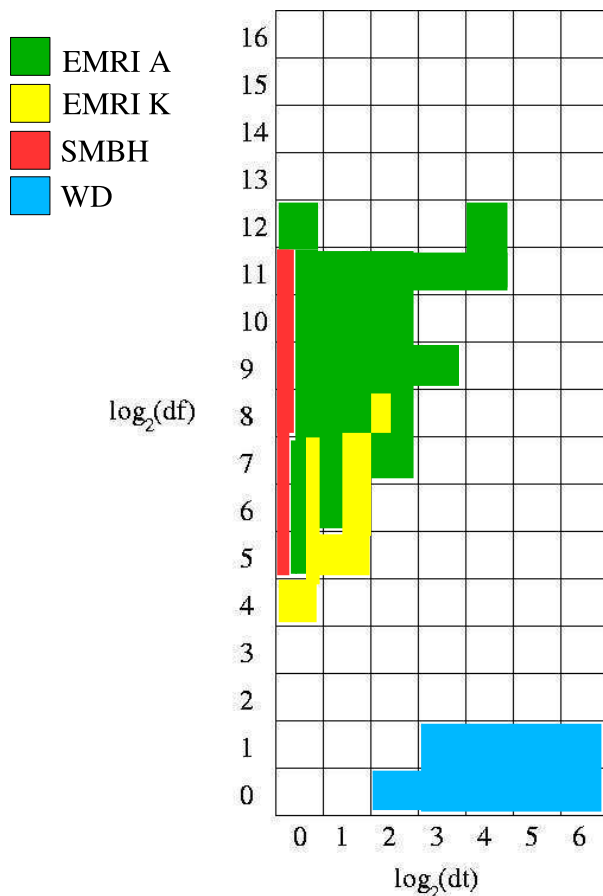


FIG. 20: Box sizes in which the majority of detections are made for various sources. For each of four different sources — EMRI “A” at 2Gpc, EMRI “K” at 2Gpc, the SMBH binary at  $z=3.125$  and the WD binary at 17kpc — we indicate all box sizes which were responsible for  $> 1\%$  of the detections of that source in 1000 realisations. The sources are colour-coded as in the key. Box sizes that were good for several sources are indicated by multiple colours.

## VII. CONCLUDING REMARKS

In this paper we have described a time-frequency algorithm, the Hierarchical Algorithm for Clusters and Ridges, that can be used to detect gravitational wave signals in LISA data. The algorithm extends the simple Excess Power search described elsewhere [9, 10] and is similar to the TFClusters algorithm used for LIGO data analysis [21]. We have investigated how the thresholds in the HACR algorithm may be tuned for specific sources and examined the performance of the algorithm for detection of three expected LISA sources — extreme mass ratio inspirals, white dwarf binaries and supermassive black hole mergers. Our results suggest that the algorithm can detect typical EMRI events at distances of up to  $\sim 2.5\text{Gpc}$ , typical WD binary events at several kpc (up to 20kpc for our favourably oriented example) and typical SMBH merger events at up to redshift  $z \sim 3.5$ . Moreover, we have demonstrated that it is possible to tune HACR to be sensitive to all three of these distinct waveform families simultaneously. This is possible because the time-frequency structure of the sources is quite different. A key ingredient of the search (as in the Excess Power search) is to bin the data using boxes of certain sizes. The time-frequency structure of the waveform family determines which boxes are well-suited to their detection, and these sets of box sizes are largely distinct for the different waveform types. This allows the overall search to be tuned for all three source families.

The HACR search includes the Excess Power search as a special case (i.e. when the pixel threshold is set equal to one). HACR must therefore perform at least as well as the Excess Power search. However, we find that the performance is not significantly better. For sources not too close to the detection limit, HACR can detect a few per cent more sources than the Excess Power algorithm. For sources at distances close to the detection limit, the HACR and Excess Power searches have very similar performance. Nonetheless, HACR represents an improvement over Excess Power since the HACR events are clusters containing several hundred pixels, rather than the single pixel identified in the Excess Power search. Parameter extraction from an Excess Power search requires a follow up stage of track identification [11]. The HACR pixel clusters, on the other hand, already directly encode information about the type of source and the source parameters. We have discussed some ways in which information can be extracted from the cluster and mapped into physical parameters, but we reserve a more in-depth discussion of this important part of the search for a future paper.

The current work contains some limitations which will also be explored in the future. The exploration of the waveform parameter space has been far from exhaustive — we have considered only a few EMRI sources, plus single examples of inspirals emitted by WD binaries and SMBH binaries. A more thorough examination of the parameter space is required to fully assess the usefulness of HACR in terms of likely LISA event rates. Our model for the LISA data stream is also somewhat simplified — we have used a low-frequency approximation, rather than the full TDI description of the detector output. While these approximations should not seriously change the conclusions, it will be important to model LISA more accurately in future studies. The most significant limitation in the current work is the fact that we have considered the extraction of a single event from noisy data. In practice, the LISA data stream will contain many thousands of events overlapping in time and frequency. The performance of HACR and other techniques will be very different under those circumstances than under the ideal conditions considered here. However, the most likely effect of source confusion will just be to limit the distance to which sources can be seen. We should still be able to identify the loudest handful of events using this or more sophisticated techniques, at considerably lower computational cost than many other approaches. The cluster properties will also provide additional information to help disentangle multiple crossing tracks. The performance of HACR in a source-dominated data stream will also be explored in the future.

In conclusion, we hope that HACR, or some similar time-frequency technique, will be able to provide a computationally cheap first stage in a hierarchical search of LISA data. The parameter estimates obtained from the clusters can be used as input for subsequent follow up with matched filtering or Markov Chain Monte Carlo techniques. This should allow detection of the loudest  $\sim 10\text{s}$  of LISA events for a very low computational overhead.

### Acknowledgments

We thank Stanislav Babak, Bangalore Sathyaprakash and R Balasubramanian for useful discussions. This work was supported by St. Catharine’s College, Cambridge (JG) and by the School of Physics and Astronomy, Cardiff University (GJ).

## APPENDIX A: STATISTICS OF TUNING

In this appendix we discuss bias that could arise in the results if the tuning is not done carefully. The tuning procedure involves first determining the optimal threshold combination for detection of a given source and then

measuring the detection rate for that threshold pair. The optimal threshold combination may be found by constructing a sequence of realisations of noise plus injected signal, analysing them with every possible threshold pair and then choosing the pair that yields the maximum detection rate. The detection rate for that optimal pair could then be taken to be the value of the rate at the observed peak. This would yield the correct rate if we were considering an extremely large number of noise realisations, but when using only a few thousand realisations, this process skews the detection rate towards artificially high numbers. Indeed, the search could be tuned for pure noise, i.e., with no injected signal. However, in a finite number of noise realisations, random fluctuations make it likely that one combination of thresholds will do unusually well for detecting those particular noise realisations. The ‘‘optimal tuned rate’’ will therefore exceed the false alarm probability, even in the absence of a signal. We discuss this more carefully in the next subsection.

### 1. Tuning to noise

In the search, we choose to assign equal false alarm probability to each box size used. The search may therefore be characterised by a single number,  $p$ , the value of the AFAP for a single box size. This number determines the search OFAP or vice versa. As defined earlier, AFAP is the false alarm rate contributed by a single box size, while OFAP is the overall false alarm rate of the entire search, including all box sizes. A choice of  $p$  determines a one parameter family of thresholds,  $(N_p^{n,l}(\eta_{up}^{n,l}), \eta_{up}^{n,l})$ , for each box size  $n \times l$ , such that the probability a cluster is found exceeding these thresholds in that binned distribution is equal to  $p$ , i.e.,

$$P(N_p > N_p^{n,l}(\eta_{up}^{n,l}), \eta_{up} > \eta_{up}^{n,l}) = p. \quad (\text{A1})$$

We assume that we know the probability distribution function of the search accurately, i.e., we can determine these thresholds precisely (e.g., having performed a sufficiently large Monte Carlo simulation). Suppose that we then tune the search for a set of signal realisations which are actually pure noise (or contain an extremely faint signal) and take the detection rate to be the maximum rate observed over all the threshold pairs for these realisations. If we used sufficiently many realisations, the result would be a detection rate that equals the assigned false alarm rate. However, tuning selects the threshold combination that maximises the event rate and is quite sensitive to random noise fluctuations. If there are  $M$  realisations of noise, we want to estimate how biased this tuning will make the detection rate, or equivalently how large  $M$  must be in order to avoid this problem.

For simplicity, we initially consider a search that uses only one box size. For a given value of the upper threshold,  $\eta_{up}^{n,l}$ , the probability that a cluster exists exceeding the threshold pair  $(N_p^{n,l}(\eta_{up}^{n,l}), \eta_{up}^{n,l})$  in a given realisation is  $p$ , by definition. Thus, the probability of a detection/no detection in a given realisation is  $p/(1-p)$ . In  $M$  realisations, the total number of detections,  $N_d$ , is therefore distributed as a binomial distribution with probability distribution.

$$P(N_d = n) = \frac{M!}{n!(M-n)!} p^n (1-p)^{(M-n)} \quad (\text{A2})$$

$$\begin{aligned} P(N_d > n) &= \sum_{m=n+1}^M \left( \frac{M!}{m!(M-m)!} p^m (1-p)^{(M-m)} \right) \\ &= \frac{B(p; n+1, M-n)}{B(n+1, M-n)} = P_{thr}(p, M, n) \end{aligned} \quad (\text{A3})$$

In this,  $B(x; a, b)/B(a, b)$  are the incomplete/complete beta functions and we use (A3) to define  $P_{thr}$ . If we considered only one threshold pair,  $(N_p^{n,l}, \eta_{up}^{n,l})$ , this would be the final story. The detection rate, defined as  $N_d/M$ , follows the binomial distribution and becomes increasingly peaked at  $N_d/M = p$  as  $M \rightarrow \infty$ . However, we consider not one threshold pair, but several. In our numerical computations, we use 100 values for the upper threshold (paired with the pixel threshold required to give the desired AFAP), but these will not all be independent. We shall suppose that there are effectively  $N_{up}$  independent choices of the upper threshold,  $\eta_{up}^{n,l}$ . When tuning the search, we take the threshold that maximizes the rate, and are therefore selecting the maximum,  $N_{max}$ , out of  $N_{up}$  independent samples. This will have the distribution

$$P(N_{max} > n) = 1 - (1 - P_{thr}(p, M, n))^{N_{up}} = 1 - P_{max}(p, M, n) \quad (\text{A4})$$

The rate measured by a single threshold,  $N_d/M$ , follows the distribution (A2) and as  $M$  is increased, this becomes increasingly peaked about  $N_d/M = p$ . In fact, from the mean and variance of  $N_d$  we obtain the mean and variance of the rate,  $N_d/M$ , measured by a single threshold

$$\langle N_d \rangle = M p \quad \Rightarrow \quad \left\langle \frac{N_d}{M} \right\rangle = p \quad (\text{A5})$$

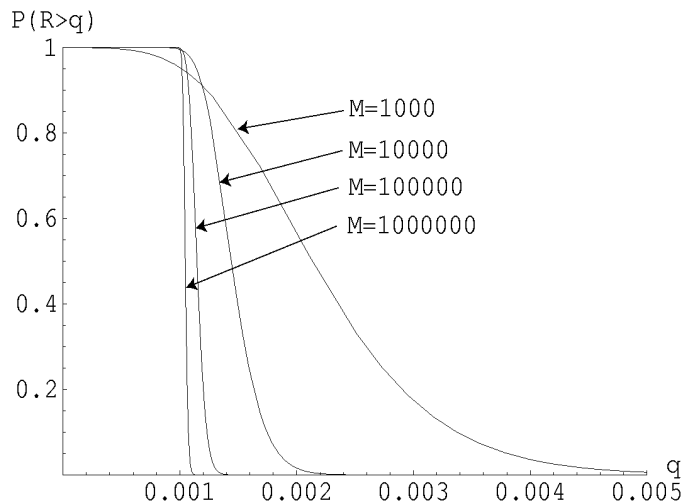


FIG. 21: Probability that the maximum rate detected out of  $N_{up} = 10$  threshold choices,  $R$ , exceeds the value  $q$ , given on the horizontal axis. The figure shown assumes a false alarm probability of  $p = 0.001$ , and  $M = 1000, 10000, 100000$  or  $1000000$  noise realisations, as labelled.

$$\text{var}(N_d) \equiv \langle (N_d - \langle N_d \rangle)^2 \rangle = M p (1 - p) \quad \Rightarrow \quad \text{var} \left( \frac{N_d}{M} \right) = \frac{1}{M} p (1 - p) \quad (\text{A6})$$

The standard deviation falls off like  $1/\sqrt{M}$ , implying the distribution becomes increasingly peaked near the mean,  $p$ . The distribution of the maximum over all the threshold choices,  $N_{max}$ , behaves similarly, although it is less strongly peaked for any given  $M$ . The distribution is illustrated in Figure 21 for a representative case with  $p = 0.001$ ,  $N_{up} = 10$  and several different choices for the number of realisations,  $M$ . For  $M = 1000$ , the distribution resembles a step function but the step is not particularly steep, and the fall off occurs above  $q = 0.001$ . As the number of realisations is increased, the step becomes sharper and moves towards  $q = p = 0.001$ . For  $M = 1000$ , there is approximately a 50% chance that the measured rate,  $N_d/M$  is more than 0.00215, or 115% above the FAP,  $p$ . To ensure a 50% or lower chance that the rate is more than 100%, 50%, 10%, 5% or 1% above the FAP, we require more than 1450, 7650, 218000, 885000 or 22400000 noise realisations respectively. To generate a reasonable ROC curve, we would need the measured rate to be within a few per cent of the FAP,  $p$ . It is clear that this is computationally impractical.

In the preceding paragraphs, we were considering only one box size. In practice, we have 119 box sizes, and we choose thresholds to maximise the rate in each box size independently. If the box sizes were independent, the distribution for each box size would follow the above relations. The overall rate is the sum of the rates in each box size, and can therefore be determined as the sum of 119 independent identically distributed (IID) random variables. However, in practice, the box sizes are not all independent. The true distribution is complicated, and must be determined numerically. However, we can say that if  $N_{box} < 119$  of the box sizes are effectively independent, the variance will be reduced by a factor of  $\sqrt{N_{box}}$ , and therefore this distribution will be more peaked than the single box size distribution. The true distribution can be derived from Monte Carlo simulations. In Figure 22 we show the ROC obtained when the search is tuned for 1000, 2000, 5000 and 10000 noise realisations. Even with 10000 noise realisations, we are still some way from the true random limit.

## 2. Determining accurate ROC curves

It is clear from the previous discussion that if we wanted to use the same set of realisations to determine the optimal threshold pair and the detection rate, then the number of realisations that must be considered is computationally prohibitive. For this reason, we tried two alternative approaches to generate ROC curves. One approach was to use the same set of noise realisations to characterize the noise (false alarm probability) and the signal (detection rate). This ensures any enhancement in the detection rate is due to the presence of the signal, and that the random search limit (i.e., detection rate equal to false alarm probability) is reached when no signal is injected. This approach should determine the optimal threshold choice quite well, but there is a bias in the detection rates it predicts since in a given set of noise realisations, there is some chance that the noise will be unusually low for a particular combination of

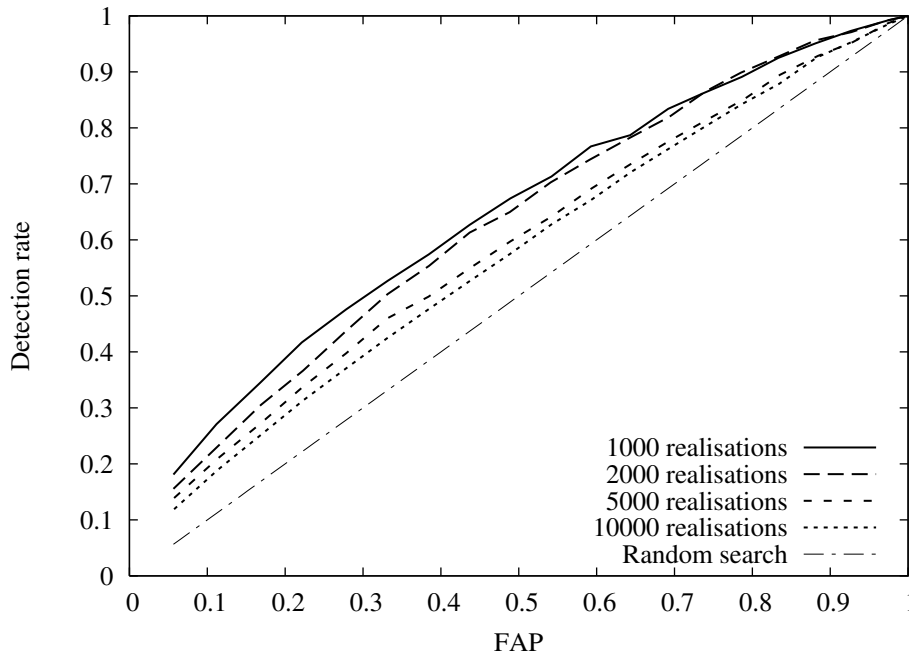


FIG. 22: Effect of bias when using a finite number of realisations for tuning. This figure shows the ROC curve obtained when tuning the search using a finite number of pure noise realisations. The number of realisations used for each line is listed in the key. We also show the random search limit, detection rate = false alarm probability, which these ROC curves should approach as the number of realisations used is increased.

thresholds. The detection rate will be artificially enhanced for such threshold combinations. A second, alternative, approach is to use one set of signal injections to determine the optimal combination of thresholds via the above procedure, and then search a second set of injections using those thresholds to determine the overall detection rate.

In Figure 23 we show ROC curves for the detection of the EMRI source “A” at a distance of 2Gpc, computed in various ways. We see from this plot that, as expected, using the same set of signal injections to choose the optimal threshold combination and measure the rate yields a noticeable overestimate of the detection rate. The problem is ameliorated somewhat if this is done using the same set of noise realisations for both the false alarm probability determination and the signal injections. Using only 2000 points, this second method also yields an overestimate of the true rate, but once the number of realisations reaches 10000, the rate appears to be approaching the true value. Using different sets of noise realisations for all three stages of the procedure yields a fair approximation to the true ROC curve. This is clear from the fact that no matter how many realisations were used in the threshold determination or rate measurement, the ROC curves all lie in roughly the same place, with a scatter of a couple of percent at most. We repeated this procedure using many different numbers of realisations at each stage of the procedure. Not all of the results are shown in Figure 23, but the other ROC curves lay in the same range in all cases. It is clear that ROC curves that are accurate to a few per cent can be obtained by tuning the threshold using one set of 1000 signal injections, and then measuring the rate using a second set of 1000 signal injections. All the ROC curves in this paper were obtained in this way.

## REFERENCES

- 
- [1] Freitag M 2001 *Class. Quantum Grav.* **18** 4033
  - [2] Gair J R, Barack L, Creighton T, Cutler C, Larson S L, Phinney E S and Vallisneri M 2004 *Class. Quantum Grav.* **21** S1595
  - [3] Cutler C 1998 *Phys. Rev. D* **57** 7089
  - [4] Barack L and Cutler C 2004 *Phys. Rev. D* **69** 082005

- [5] Cornish N J and Crowder J 2005 *Phys. Rev. D* **72** 043005
- [6] Umstätter R, Christensen N, Hendry M, Meyer R, Simha V, Veitch J, Vigeland S and Woan G 2005 *Phys. Rev. D* **72** 022001
- [7] Wickham E D L, Stroeer A and Vecchio A 2006 preprint gr-qc/0605071
- [8] Stroeer A, Gair J R and Vecchio A 2006 preprint gr-qc/0605227
- [9] Wen L and Gair J R, *Class. Quantum Grav.* **22** S445 (2005)
- [10] Gair J R and Wen L, *Class. Quantum Grav.* **22** S1359 (2005)
- [11] Wen L, Chen, Y and Gair J R, Proceedings of 6th LISA Symposium, submitted
- [12] Heng I S, Balasubramanian R, Sathyaprakash B S and Schutz B F, *Class. Quantum Grav.* **21** S821 (2004)
- [13] Danzmann K et al. 1998 *LISA - Laser Interferometer Space Antenna, Pre-Phase A Report*, Max-Planck-Institut für Quantenoptik Report MPQ 233
- [14] Vallisneri M 2005 *Phys. Rev. D* **72** 042003
- [15] Sesana A, Haardt F, Madau P and Volonteri M 2005 *Astrophys. J.* **623** 23
- [16] Volonteri M, Madau P, Quartet E and Rees M J, 2005, *Astrophys. J.*, 620, 69
- [17] Miniutti G, Fabian A C and Miller J, 2005, *Mon. Not. Roy. Astron. Soc.* , 351, 466
- [18] Fabian A C, Miniutti G, Iwasawa K and Ross R R, 2005, *Mon. Not. Roy. Astron. Soc.* , 361, 795
- [19] Babak S V, Fang H, Gair J R, Glampedakis K and Hughes S A, 2006 preprint gr-qc/0607007
- [20] Gair J R and Glampedakis K (2006) *Phys. Rev. D* **73** 064037
- [21] Sylvestre J, *Phys. Rev. D* **66** 102004 (2002)
- [22] Stroeer A and Vecchio A, 2006 preprint gr-qc/0605227
- [23] Sahní V, Sathyaprakash B S and Shandarin S F, *Astrophys. J.*, 495, L5 (1998)

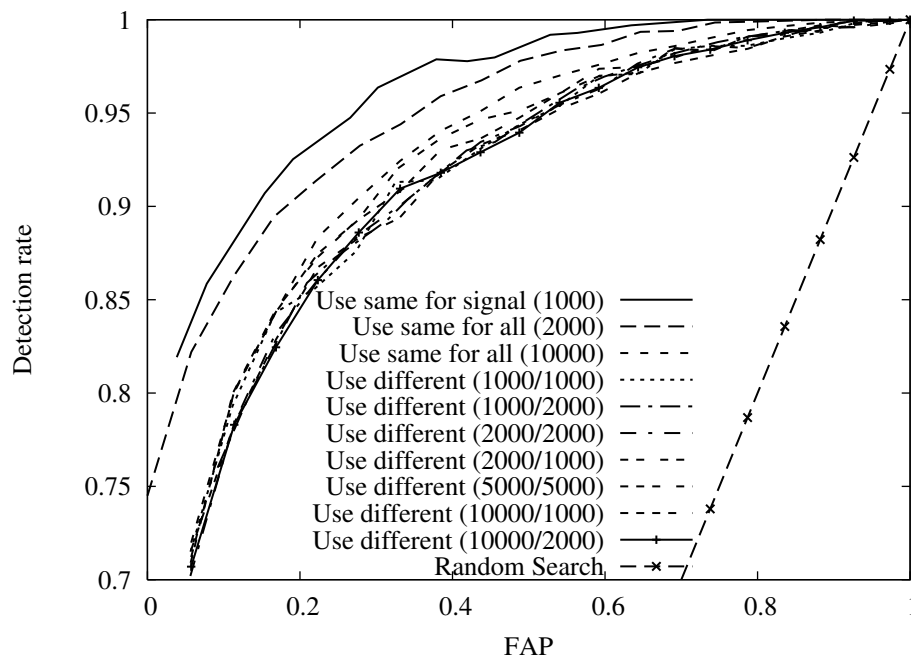


FIG. 23: Illustration of potential bias in ROC determination. We show several ROC curves for the detection of source “A” at a distance of 2Gpc using HACR. In each case, the ROC curve was computed as outlined in the text — a set of pure noise realisations were used to determine a one parameter family of thresholds corresponding to a given overall false alarm probability (FAP), a set of injections of the signal into noise were used to determine the combination of thresholds that gave the maximum detection rate at that FAP and then a set of signal injections were used to determine the detection rate using the optimal threshold combination. Curves labelled by “Use different” used different sets of noise realisations for each of the three stages. The numbers in brackets are the number of realisations used for choosing the optimal threshold pair and for measuring the detection rate. All curves used 10000 noise realisations for determining the FAP. The curve labelled “Use same for signal” used the same set of injections for determining the optimal threshold pair and the rate. The curves labelled “Use same for all” used the same set of noise realisations for all three stages, with the number of realisations given in brackets.